New 5 flavor next-to-leading-order analysis and parametrizations of parton distributions of the real photon

F. Cornet

Departamento de Física Teórica y del Cosmos, Universidad de Granada, Campus de Fuente Nueva, E-18071, Granada, Spain and Centro Andaluz de Física de Partículas elementales (CAFPE), Campus de Fuente Nueva, E-18071 Granada, Spain

P. Jankowski and M. Krawczyk

Institute of Theoretical Physics, Warsaw University, ulica Hoża 69, 00-681 Warsaw, Poland

(Received 8 May 2004; published 9 November 2004)

New, radiatively generated, next-to-leading (NLO) quark (u, d, s, c, b) and gluon densities in a real, unpolarized photon are presented. We perform three global fits, based on the NLO Dokshitzer-Gribov-Lipatov-Altarelli-Parisi evolution equations for $Q^2 > 1$ GeV^2, to all the available structure-function $F_2^\gamma(x, Q^2)$ data. As in our previous LO analysis we utilize two theoretical approaches. Two models, denoted as FFNS$_{\rm CJK}1$ and FFNS$_{\rm CJK}2$ NLO, adopt the so-called fixed flavor-number scheme for calculation of the heavy-quark contributions to $F_2^\gamma(x, Q^2)$; the Cornet-Jankowski-Krawczyk NLO model applies the ACOT(χ) scheme. We examine the results of our fits by a comparison with the LEP data for the Q^2 dependence of the F_2^γ, averaged over various x regions, and the $F_{2,c}^\gamma$. Grid parametrizations of the parton densities for all fits are provided.

DOI: 10.1103/PhysRevD.70.093004 PACS numbers: 14.70.Bh, 13.60.Hb, 14.65.Dw, 14.65.Fy

I. INTRODUCTION

In this work we extend the leading order (LO) QCD analysis of the structure function $F_2^\gamma(x, Q^2)$ of the unpolarized real photon [1–3], to the next-to-leading order (NLO). As before we are especially interested in the description of the charm- and beauty-quark contributions to $F_2^\gamma(x, Q^2)$. We adopt two approaches, the fixed flavor-number scheme (FFNS$_{\rm CJK}$) and Cornet, Jankowski, and Krawczyk (CJK) ones, as discussed in [1] and (with some modifications) in [2]. In the first model, referred to as FFNS$_{\rm CJK}1$ NLO, we adopt a standard approach in which a heavy quark, h, contributes to the photon structure function only through the "direct" (Bethe-Heitler) $\gamma^* + \gamma \to h + \bar{h}$ process and the process with "resolved photon" $\gamma^* + G^\gamma \to h + \bar{h}$. In the FFNS$_{\rm CJK}2$ NLO model we include in addition $\gamma^* + G^\gamma \to h + \bar{h} + G$ and $\gamma^* + q^\gamma(\bar{q}^\gamma) \to q(\bar{q}) + h + \bar{h}$ processes [4]. In the third model, CJK NLO, we use the ACOT(χ) scheme [5] in which, apart from the direct and resolved-photon $O(\alpha_s)$ contributions [6], we deal with the heavy-quark densities $q_h(x, Q^2)$. The subtraction of the double counted terms as well as introduction of a new kinematic variable χ_h improves the description of $F_2^\gamma(x, Q^2)$ in both regions: below and above the heavy-quark thresholds.

In [1–3] we followed the idea of the radiatively generated parton distributions introduced by the Glück, Reya, Vogt (GRV) group first to describe nucleon [7] and pion [8] and later used for the real [9,10] and virtual photon [10,11]. In our LO analyses [1–3] we used $Q_0^2 = 0.25$ GeV^2 and adopted the input distributions of the valence-type form introduced in [9] neglecting sea-quark densities. In the case of the NLO analysis we found that the starting scale of the evolution appears to tend to higher values, $Q_0^2 \approx 0.7$ GeV^2 (similarly as in [12]). We tested the assumption on vanishing sea-quark densities at Q_0^2 by performing additional fits.

All our global fits are performed at $Q^2 > 1$ GeV^2 utilizing the set of all available $F_2^\gamma(x, Q^2)$ data.

We test our results for $F_2^\gamma(x, Q^2)$ by comparing them with the LEP data which were not used in the fits: for the Q^2 dependence of the F_2^γ, averaged over various x regions, and for the charm contribution to the structure-function, $F_{2,c}^\gamma$, data.

Our paper is divided into six parts. In Sec. II we shortly recall the basic schemes applied to the calculation of the heavy-quark production in the deep inelastic scattering (DIS) on a real-photon target. Section III is devoted to the description of the FFNS$_{\rm CJK}$ NLO models of the $F_2^\gamma(x, Q^2)$. Next, the CJK NLO model based on the ACOT(χ) scheme [5] is presented in detail. In Sec. IV we describe the solutions of the Dokshitzer-Gribov-Lipatov-Altarelli-Parisi (DGLAP) evolution equations in all models and assumptions for the input parton densities. Results of the global fits are discussed and compared with the $F_2^\gamma(x, Q^2)$, $F_2^\gamma(Q^2)$, and $F_{2,c}^\gamma$ data in the fifth section of the paper. We end our paper by presenting in the Appendix the technical details of the calculation. The parton distributions resulting from our fits have been parametrized on a grid in (x, Q^2).

II. PRODUCTION OF HEAVY QUARKS IN DIS$_{e\gamma}$

The deep inelastic scattering on a photon (DIS$_{e\gamma}$) allows one to measure the structure function F_2^γ, and others, via the process

$$e + \gamma \to e + \text{hadrons}, \tag{1}$$

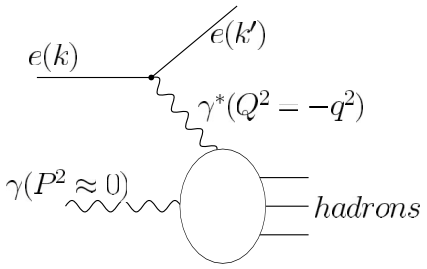

FIG. 1. Deep inelastic scattering on quasireal photon ($P^2 \approx 0$), $e + \gamma \to e +$ hadrons.

presented in Fig. 1. The differential cross section for this process is given by

$$\frac{d\sigma^{e\gamma\to eX}}{dxdy} = \frac{2\pi\alpha^2}{xyQ^2}\{[1 + (1 - y)^2]F_2^\gamma(x, Q^2) - y^2 F_L^\gamma(x, Q^2)\}, \quad (2)$$

where x and y are the standard $\mathrm{DIS}_{e\gamma}$ variables, defined through the virtuality Q^2 of the probing photon and momenta of interacting particles shown in Fig. 1,

$$x = \frac{Q^2}{2p \cdot q}, \qquad y = \frac{p \cdot q}{p \cdot k}, \quad (3)$$

and $F_L^\gamma(x, Q^2)$ is the so-called longitudinal structure function corresponding to the exchange of the longitudinally polarized γ^*. For the presently kinematically accessible values of y the $F_L^\gamma(x, Q^2)$ contribution is negligible.

Each of the partons (quarks and gluon) of the real photon contributes to the $F_2^\gamma(x, Q^2)$ proportionally to the corresponding partonic cross section. The calculation of the light u-, d-, s-quark and gluon cross sections is straightforward.

Various schemes used in the calculation of the heavy-quark production have been described in [1]. They are also explained in the vast literature, [5,13,14]. Let us shortly recall the main facts on the FFNS and ACOT(χ) approaches applied in this analysis.

There exist two standard schemes in a calculation of a heavy-quark, h, production at the hard scale μ. In both of them the light quarks u, d, and s are treated as massless because for them $\mu \gg \Lambda_{\mathrm{QCD}} > m_q$, where m_q is a light-quark mass. In the case of the DIS process the hard scale μ is identified with the virtuality of the probing photon, $\mu^2 = Q^2$. In the massive FFNS heavy c and b quarks are treated differently: the massive charm and beauty quarks produced in hard subprocesses $\gamma^* + \gamma \to h + \bar{h}$ can appear only in the final state. In the second, massless scheme, called the zero-mass variable flavor-number scheme (ZVFNS), heavy-quark distributions appear similar to the light-parton densities. When Q^2 is larger than a threshold associated with a heavy quark (usually taken as $Q^2 = m_h^2$), this quark is considered as an extra massless parton in addition to the three light quarks. This way, the number of different types of quarks (flavors) increases with increasing Q^2. One introduces a notion of "active quarks," for which the condition $Q^2 > m_q^2$ is fulfilled and which can be treated as massless partons of the probed real photon. When active, their densities $q_i(x, Q^2)$ differ from zero, otherwise $q_i(x, Q^2) = 0$.

The above standard schemes are considered to be reliable in different Q^2 regions. The FFNS loses its descriptive power when $Q^2 \gg m_h^2$; on the other hand the ZVFNS does not seem appropriate if $Q^2 \approx m_h^2$. To obtain a prescription working for all hard scales one needs to combine features of both schemes. There exists a whole set of approaches, generally denoted as general-mass variable flavor-number schemes (GVFNS), which in the $Q^2 \to m_h^2$ and $Q^2 \to \infty$ limits reproduce the behavior of the FFNS and ZVFNS schemes, respectively. Their recent realization is the so-called ACOT(χ) scheme introduced for the proton structure function in [5] and used by us in our LO analysis [1–3].

In the ACOT(χ) scheme, all contributions to the considered process, which would be included separately in the ZVFNS and FFNS, are taken into account. Such a procedure requires proper subtraction of double counted contributions, i.e., the large logarithms which appear in the massive heavy-quark Wilson coefficients (the FFNS scheme) that are also resummed in the $q_h(x, \mu^2)$ densities. That way one obtains a scheme in principle appropriate in the whole Q^2 range. Still, another problem emerges. In any process the kinematical threshold for the heavy-quark production is given by the total energy of that process, W. Obviously W must be greater than twice the mass of the heavy quark in hand, $W > 2m_h$, so in the $\mathrm{DIS}_{e\gamma}$ case where the hard scale is Q^2, we have $W^2 = (1 - x)Q^2/x > 4m_h^2$. As $\mu^2 = Q^2$ the ZVFNS condition $\mu > m_h$ (or any similar) for treating a heavy quark h as a massless parton is not correct. It may happen (for small enough x) that $q_h(x, Q^2) = 0$ in the kinematically allowed region $W > 2m_h$. On the other hand, we can also obtain nonzero heavy-quark densities in the kinematically forbidden (x, Q^2) region. The ACOT(χ) scheme solves this problems through the introduction of a new variable $\chi_h \equiv x(1 + 4m_h^2/Q^2)$ which replaces in the ZVFNS the Bjorken x as an argument of the heavy-parton density.

In the next sections we will present the realizations of the FFNS and ACOT(χ) schemes for the calculation of the photon structure F_2^γ in the next-to-leading order of QCD, namely, our $\mathrm{FFNS}_{\mathrm{CJK}}$ NLO and CJK NLO models.

III. DESCRIPTION OF THE F_2^γ IN THE $\mathrm{FFNS}_{\mathrm{CJK}}$ NLO

This section is devoted to the $\mathrm{FFNS}_{\mathrm{CJK}}1$ and $\mathrm{FFNS}_{\mathrm{CJK}}2$ NLO models, which are the realizations of the FFNS approach for the photon structure F_2^γ in the next-to-leading order of QCD. The only difference between these two models is that the $\mathrm{FFNS}_{\mathrm{CJK}}$ NLO 2 approach includes

additional higher order contributions to F_2^γ neglected in the $\mathrm{FFNS_{CJK}}$ NLO 1 model.

First, we describe the light-quark contributions to $F_2^\gamma(x, Q^2)$ which are common for both analyzed models. Next, we discuss the heavy-quark contributions for the $\mathrm{FFNS_{CJK}}$ NLO approach. Further, we recall the DIS_γ factorization scheme used in the model and resume by giving the final formulas for $F_2^\gamma(x, Q^2)$ in the $\mathrm{FFNS_{CJK}}$ NLO models.

A. Light-quark contributions

In the next-to-leading-order logarithmic approximation of QCD or, in short, in NLO QCD the light-quark contributions to the photon structure function $F_2^\gamma(x, Q^2)$ can be written in terms of light-quark (u, d, and s) densities $q_i^\gamma(x, Q^2)$ as follows:

$$\frac{1}{x}F_2^\gamma(x,Q^2)|_{\mathrm{light}} = \sum_{i=1}^{3} e_i^2 \Big\{ (q_i^\gamma + \bar{q}_i^\gamma)(x,Q^2) + e_i^2 \frac{\alpha}{2\pi} C_{2,\gamma}^{(0)}(x) + \frac{\alpha_s(Q^2)}{2\pi} \int_x^1 \frac{dy}{y} \Big[(q_i^\gamma + \bar{q}_i^\gamma)(y,Q^2) \times C_{2,q}^{(1)}\Big(\frac{x}{y}\Big) + G^\gamma(y,Q^2) C_{2,G}^{(1)}\Big(\frac{x}{y}\Big) \Big] \Big\}. \quad (4)$$

Note that $q_i^\gamma(x, Q^2) = \bar{q}_i^\gamma(x, Q^2)$. The $C_{2,j}^{(i)}(x)$ functions are the $O(\alpha_s^i)$ order terms of the hadronic (Wilson) coefficient functions ($j = \gamma, q, G$)

$$C_{2,j}(x,Q^2) = C_{2,j}^{(0)}(x) + \frac{\alpha_s(Q^2)}{2\pi} C_{2,j}^{(1)}(x) + \cdots. \quad (5)$$

Each of them is related to the hard process of a parton originating from the real photon [for instance, quark for $C_{2,q}(x)$] interacting with the virtual photon. The relevant processes for each coefficient appearing in Eq. (4) are shown in Table I. The formulas for the $C_{2,j}^{(i)}(x)$ functions up to $O(\alpha_s^2)$ can be found in [15]; see also the Appendix.

The evolution of the parton densities in $\ln Q^2$ is governed by the inhomogeneous DGLAP equations [16]. In the NLO we have

TABLE I. Hard parton processes and the corresponding Wilson-coefficient functions for light quarks.

Order	Hard (parton) process	Coefficient function
$O(\alpha_s^0)$	$\gamma^* + q^\gamma(\bar{q}^\gamma) \to q(\bar{q})$	$C_{2,q}^{(0)}(x) = \delta(1-x)$
	$\gamma^* + \gamma \to q + \bar{q}$	$C_{2,\gamma}^{(0)}(x)$
$O(\alpha_s^1)$	$\gamma^* + q^\gamma(\bar{q}^\gamma) \to q(\bar{q}) + G$	$C_{2,q}^{(1)}(x)$
	$\gamma^* + G^\gamma \to q + \bar{q}$	$C_{2,G}^{(1)}(x)$

$$\frac{dq_i^\gamma(x,Q^2)}{d\ln Q^2} = \frac{\alpha}{2\pi} e_i^2 k_q(x,Q^2) + \frac{\alpha_s(Q^2)}{2\pi} \int_x^1 \frac{dy}{y} \times \Big\{ \sum_{k=1}^{N_f} \Big[q_k^\gamma(y,Q^2) P_{qq}\Big(\frac{x}{y},Q^2\Big) + \bar{q}_k^\gamma(y,Q^2) P_{q\bar{q}}\Big(\frac{x}{y},Q^2\Big) \Big] + G^\gamma(y,Q^2) P_{qG}\Big(\frac{x}{y},Q^2\Big) \Big\}, \quad (6)$$

$$\frac{dG^\gamma(x,Q^2)}{d\ln Q^2} = \frac{\alpha}{2\pi} k_G(x,Q^2) + \frac{\alpha_s(Q^2)}{2\pi} \int_x^1 \frac{dy}{y} \times \Big\{ \sum_{k=1}^{N_f} \Big[q_k^\gamma(y,Q^2) P_{Gq}\Big(\frac{x}{y},Q^2\Big) + \bar{q}_k^\gamma(y,Q^2) P_{G\bar{q}}\Big(\frac{x}{y},Q^2\Big) \Big] + G^\gamma(y,Q^2) P_{GG}\Big(\frac{x}{y},Q^2\Big) \Big\}, \quad (7)$$

where N_f is the number of active quarks. Here $N_f = 3$ as all heavy-quark densities are equal to zero in the FFNS models. The functions $P_{ij}(x, Q^2)$ and $k_i(x, Q^2)$ are the NLO splitting functions

$$k_i(x,Q^2) = k_i^{(0)}(x) + \frac{\alpha_s(Q^2)}{2\pi} k_i^{(1)}(x), \qquad P_{ij}(x,Q^2) = P_{ij}^{(0)}(x) + \frac{\alpha_s(Q^2)}{2\pi} P_{ij}^{(1)}(x). \quad (8)$$

The $k_q(x, Q^2)$ and $k_G(x, Q^2)$ are referred to as the photon-quark and photon-gluon splitting functions, respectively. Up to the NLO order $P_{Gq} = P_{G\bar{q}}$. Formulas for $O(\alpha_s)$ and $O(\alpha_s^2)$ splitting functions can be found for instance in [17].

B. Heavy-quark contributions

In the FFNS models heavy quarks appear only in the final state of the process and the density functions $q_h(x, Q^2)$ are equal to zero. The charm- and beauty-quark contributions to the structure function are described by the heavy-quark coefficient functions $C_{2,j}^{h,(i)}$ related to the hard processes as listed in Table II. One obtains

TABLE II. Hard parton processes and the corresponding Wilson-coefficient functions for heavy quarks.

Order	Parton subprocess	Coefficient function
$O(\alpha_s^0)$	$\gamma^* + \gamma \to h + \bar{h}$	$C_{2,\gamma}^{h,(0)}$
$O(\alpha_s^1)$	$\gamma^* + G^\gamma \to h + \bar{h}$	$C_{2,G}^{h,(1)}$
	$\gamma^* + \gamma \to h + \bar{h} + G$	$C_{2,\gamma}^{h,(1)}$
$O(\alpha_s^2)$	$\gamma^* + G^\gamma \to h + \bar{h} + G$	$C_{2,G}^{h,(2)}$
	$\gamma^* + q^\gamma(\bar{q}^\gamma) \to q(\bar{q}) + h + \bar{h}$	$C_{2,q}^{h,(2)}$, $C_{2,q}^{(2)}$

$$\frac{1}{x}F_2^\gamma(x,Q^2)|_{\text{heavy,FFNS}} = \sum_{h(=c,b)}^{2}\Big\{e_h^4\Big[\frac{\alpha}{2\pi}C_{2,\gamma}^{h,(0)}\Big(x,\frac{Q^2}{m_h^2}\Big)+\frac{\alpha\alpha_s(Q^2)}{(2\pi)^2}C_{2,\gamma}^{h,(1)}\Big(x,\frac{Q^2}{m_h^2}\Big)\Big]$$
$$+e_h^2\Big[\frac{\alpha_s(Q^2)}{2\pi}\int_{\chi_h}^1\frac{dy}{y}G^\gamma(y,Q^2)C_{2,G}^{h,(1)}\Big(\frac{x}{y},\frac{Q^2}{m_h^2}\Big)+\Big(\frac{\alpha_s(Q^2)}{2\pi}\Big)^2\int_{\chi_h}^1\frac{dy}{y}G^\gamma(y,Q^2)C_{2,G}^{h,(2)}\Big(\frac{x}{y},\frac{Q^2}{m_h^2}\Big)\Big]$$
$$+\Big(\frac{\alpha_s(Q^2)}{2\pi}\Big)^2\int_{\chi_h}^1\frac{dy}{y}\sum_{i=1}^{3}(q_i^\gamma+\bar{q}_i^\gamma)(y,Q^2)\Big[e_i^2C_{2,q}^{(2)}\Big(\frac{x}{y},\frac{Q^2}{m_h^2}\Big)+e_h^2C_{2,q}^{h,(2)}\Big(\frac{x}{y},\frac{Q^2}{m_h^2}\Big)\Big]\Big\}, \quad (9)$$

where the parameter $\chi_h = x(1+4m_h^2/Q^2)$ takes care of the proper region of the integration.

We consider two FFNS models, $\text{FFNS}_{\text{CJK}}1$ and $\text{FFNS}_{\text{CJK}}2$ NLO, where only in the latter we include the $O(\alpha_s^2)$ and $O(\alpha\alpha_s)$ contributions to F_2^γ. The reason for considering two models is twofold. First, to check the size of the higher order heavy-quark contributions. Second, to perform a test whether the $O(\alpha_s^2)$ and $O(\alpha\alpha_s)$ terms should be included in the calculations as they are of higher order than the other NLO contributions.

Let us notice that among the higher order terms there appear two Wilson coefficients originating from the process $\gamma^* + q^\gamma(\bar{q}^\gamma) \to q(\bar{q}) + h + \bar{h}$, the $C_{2,q}^{h,(2)}$ and $C_{2,q}^{(2)}$ (see Fig. 2), the interference term of two diagrams (proportional to $e_h e_q$) gives 0 according to [15].

C. The $\overline{\text{MS}}$ and DIS_γ factorization schemes

All the splitting and coefficient functions introduced in former sections have been derived in the modified minimal subtraction factorization scheme ($\overline{\text{MS}}$). (They all can be found in the literature, see the Appendix.) Let us notice that the $C_{2,\gamma}^{(0)}(x)$ term in Eq. (4), describing the direct contribution of the photon to $F_2^\gamma(x,Q^2)$, causes a problem in the $\overline{\text{MS}}$ scheme [18]. First, contrary to all other contributions, this term does not vanish at the input scale Q_0^2. One obtains very different boundary conditions for the light-quark contribution in LO and NLO:

$$\frac{1}{x}F_2^\gamma(x,Q_0^2)|_{\text{light}} = \begin{cases} 0, & \text{LO}, \\ \sum_{i=1}^3 e_i^4\frac{\alpha}{2\pi}C_{2,\gamma}^{(0)}(x), & \text{NLO}. \end{cases} \quad (10)$$

This leads to very distinct results over the whole x range (see for instance [19]). The heavy-quark contributions, $C_{2,\gamma}^{h,(k)}[x,(Q^2/m_h^2)]$, for $k=0$, 1, of Eq. (9) do not cause a similar problem as the $O(\alpha_s^0)$ term appears already in the LO calculation and the $C_{2,\gamma}^{h,(1)}[x,(Q^2/m_h^2)]$ coefficient is only its $O(\alpha_s^1)$ correction.

Secondly, the $C_{2,\gamma}^{(0)}(x)$ term calculated in the $\overline{\text{MS}}$ scheme is negative and divergent in the large-x region, where $C_{2,\gamma}^{(0)}(x) \simeq 3[\ln(1-x)-1]$, leading to unphysical negative values of F_2^γ at $x \to 1$. It is not cured by the addition of other NLO contributions to the structure function as they all vanish at $x=1$ (if a typical choice of the shape of the hadronic input is made).

In a new factorization scheme, denoted as DIS_γ, introduced in [18], one avoids the troubles connected with the $C_{2,\gamma}^{(0)}(x)$ term by absorbing it into the quark distributions $q_i^\gamma(x,Q^2)$, namely,

$$q_i^{\text{DIS}_\gamma}(x,Q^2) = q_i^{\overline{\text{MS}}}(x,Q^2) + e_i^2\frac{\alpha}{4\pi}C_{2,\gamma}^{(0),\overline{\text{MS}}}(x),$$
$$C_{2,\gamma}^{(0),\text{DIS}_\gamma}(x) = C_{2,\gamma}^{(0),\overline{\text{MS}}}(x) + \Delta C_{2,\gamma}^{(0)}(x) = 0, \quad (11)$$

where obviously

$$\Delta C_{2,\gamma}^{(0)}(x) = -C_{2,\gamma}^{(0),\overline{\text{MS}}}(x). \quad (12)$$

The gluon density and other coefficient functions are unaltered by the above redefinition but it leads to a modification of the photon-quark and photon-gluon splitting functions appearing in the DGLAP evolution of the parton distributions:

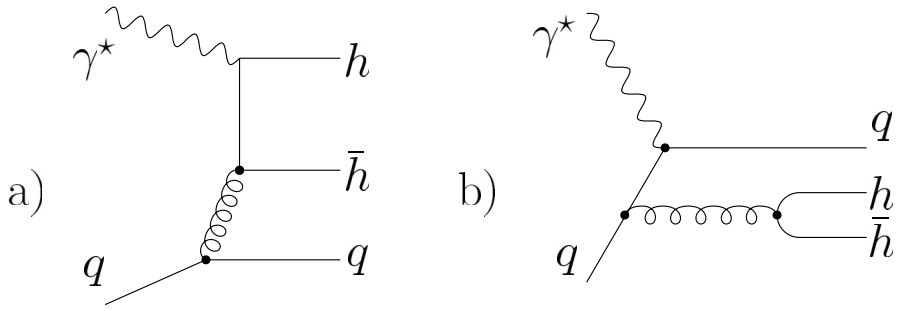

FIG. 2. Diagrams relevant for the $\gamma^* + q^\gamma(\bar{q}^\gamma) \to q(\bar{q}) + h + \bar{h}$ process corresponding to (a) the $C_{2,q}^{h,(2)}$ coefficient and (b) the $C_{2,q}^{(2)}$ coefficient.

$$k_q^{(1),\mathrm{DIS}_\gamma}(x,Q^2) = k_q^{(1),\overline{\mathrm{MS}}}(x,Q^2) - \frac{1}{2}\int_x^1 \frac{dy}{y} P_{qq}^{(0)}\left(\frac{x}{y}\right) C_{2,\gamma}^{(0),\mathrm{DIS}_\gamma}(y),$$
$$k_G^{(1),\mathrm{DIS}_\gamma}(x,Q^2) = k_G^{(1),\overline{\mathrm{MS}}}(x,Q^2) - \sum_{i=1}^{N_f} e_i^2 \int_x^1 \frac{dy}{y} P_{Gq}^{(0)}\left(\frac{x}{y}\right) C_{2,\gamma}^{(0),\mathrm{DIS}_\gamma}(y). \tag{13}$$

In our analysis we apply the DIS_γ factorization scheme;, for simplicity the DIS_γ superscript will be omitted below, if possible.

D. Formulas for F_2^γ

$F_2^\gamma(x,Q^2)$ in the $\mathrm{FFNS_{CJK}}$ NLO 1 model reads

$$\frac{1}{x}F_2^\gamma(x,Q^2)|_{\mathrm{FFNS}}1 = \sum_{i=1}^{3} e_i^2\left\{(q_i^\gamma+\bar{q}_i^\gamma)(x,Q^2) + \frac{\alpha_s(Q^2)}{2\pi}\int_x^1\frac{dy}{y}\left[(q_i^\gamma+\bar{q}_i^\gamma)(y,Q^2)C_{2,q}^{(1)}\left(\frac{x}{y}\right) + G^\gamma(y,Q^2)C_{2,G}^{(1)}\left(\frac{x}{y}\right)\right]\right\}$$
$$+\sum_{h(=c,b)}^{2} e_h^2\left\{\frac{\alpha_s(Q^2)}{2\pi}\int_{\chi_h}^1\frac{dy}{y}G^\gamma(y,Q^2)C_{2,G}^{h,(1)}\left(\frac{x}{y},\frac{Q^2}{m_h^2}\right) + e_h^2\frac{\alpha}{2\pi}C_{2,\gamma}^{h,(0)}\left(x,\frac{Q^2}{m_h^2}\right)\right\}. \tag{14}$$

In the case of the $F_2^\gamma(x,Q^2)|_{\mathrm{FFNS}}2$ model we include the $O(\alpha_s^2)$ and $O(\alpha\alpha_s)$ terms, obtaining

$$\frac{1}{x}F_2^\gamma(x,Q^2)|_{\mathrm{FFNS}}2 = \frac{1}{x}F_2^\gamma(x,Q^2)|_{\mathrm{FFNS}}1 + \sum_{h(=c,b)}^{2}\left(\frac{\alpha_s(Q^2)}{2\pi}\right)^2 e_h^4 C_{2,\gamma}^{h,(1)}\left(x,\frac{Q^2}{m_h^2}\right)$$
$$+\sum_{h(=c,b)}^{2}\left(\frac{\alpha_s(Q^2)}{2\pi}\right)^2\int_{\chi_h}^1\frac{dy}{y}\left\{\sum_{i=1}^{3}(q_i^\gamma+\bar{q}_i^\gamma)(y,Q^2)\left[e_i^2 C_{2,q}^{(2)}\left(\frac{x}{y},\frac{Q^2}{m_h^2}\right) + e_h^2 C_{2,q}^{h,(2)}\left(\frac{x}{y},\frac{Q^2}{m_h^2}\right)\right]\right.$$
$$\left.+e_h^2 G^\gamma(y,Q^2)C_{2,G}^{h,(2)}\left(\frac{x}{y},\frac{Q^2}{m_h^2}\right)\right\}. \tag{15}$$

IV. DESCRIPTION OF THE F_2^γ IN THE CJK NLO MODEL

This section is devoted to the description of the CJK NLO model based on the ACOT(χ) approach. The approach combines the FFNS scheme introduced in the former section with the ZVFNS scheme in which heavy quarks are treated in a similar way as the light ones.

A. Light-quark contributions

The light-quark contributions to F_2^γ are the same in FFNS and ZVFNS schemes and were already given in Eq. (4) for the $\overline{\mathrm{MS}}$ factorization scheme and in Eq. (14) for the DIS_γ scheme. The difference between the numerical values of those contributions originates from the difference between the number of the active quarks, N_f, in the DGLAP equations in both approaches. We have $N_f = 3$ for the $\mathrm{FFNS_{CJK}}$ NLO models, while $N_f = 5$ in the CJK NLO model.

B. Heavy-quark contributions

The heavy-quark contributions in the region $Q^2 \approx m_h^2$ are properly described by the FFNS formula, Eq. (9). Notice that in the CJK NLO model we neglect the $O(\alpha_s^2)$ and $O(\alpha\alpha_s)$ contributions because they lead to a very complicated expression for $F_2^\gamma(x,Q^2)$ and their analysis is beyond the scope of this work. In the region $Q^2 \gg m_h^2$, however, the ZVFNS is more appropriate than the FFNS. We, thus, include the ZVFNS contributions as massless charm- and beauty-quark distributions, $q_h(x,Q^2)$, in the photon. They are combined with the light-quark densities through the DGLAP equations with $N_f = 5$ active quarks. In the ZVFNS approach heavy-quark contributions to $F_2^\gamma(x,Q^2)$ read (in the $\overline{\mathrm{MS}}$ scheme)

$$\frac{1}{x}F_2^\gamma(x,Q^2)|_{\mathrm{heavy,ZVFNS}} = \sum_{h(=c,b)}^{2} e_h^2\left\{(q_h^\gamma+\bar{q}_h^\gamma)(x,Q^2) + e_h^2\frac{\alpha}{2\pi}C_{2,\gamma}^{(0)}(x)\right.$$
$$\left.+\frac{\alpha_s(Q^2)}{2\pi}\int_x^1\frac{dy}{y}\left[(q_h^\gamma+\bar{q}_h^\gamma)(y,Q^2)C_{2,q}^{(1)}\left(\frac{x}{y}\right) + G^\gamma(y,Q^2)C_{2,G}^{(1)}\left(\frac{x}{y}\right)\right]\right\}. \tag{16}$$

C. Subtraction terms

A simple summing of all the discussed terms, namely,

$$F_2^\gamma(x,Q^2) = F_2^\gamma(x,Q^2)|_{\text{light}} + F_2^\gamma(x,Q^2)|_{\text{heavy,FFNS}} + F_2^\gamma(x,Q^2)|_{\text{heavy,ZVFNS}}, \tag{17}$$

would lead to double counting of some contributions. Let us notice first that the ZVFNS subprocess with the direct coupling of the real photon to the (massless) heavy quark, term $C_{2,\gamma}^{(0)}(x)$ in Eq. (16), was also included in the FFNS formula (9) as $C_{2,\gamma}^{h,(0)}[x,(Q^2/m_h^2)]$. Those two terms originate from the same $\gamma^* + \gamma \to h + \bar{h}$ process, however they are not equal as the $C_{2,\gamma}^{(0)}(x)$ term is obtained in a massless approximation. The same is true for the $C_{2,G}^{(0)}(x)$ [Eq. (16)] and $C_{2,G}^{h,(0)}[x,(Q^2/m_h^2)]$ [Eq. (9)] terms arising from the $\gamma^* + G^\gamma \to h + \bar{h}$ process. Obviously, only one set of the above terms should be included in the final CJK NLO formula for the $F_2^\gamma(x,Q^2)$. We choose to keep the massive $C_{2,\gamma}^{h,(0)}[x,(Q^2/m_h^2)]$ and $C_{2,G}^{h,(0)}[x,(Q^2/m_h^2)]$ and discard their massless approximations from the ZVFNS because the latter do not vanish at the heavy-quark thresholds.

The massless $C_{2,\gamma}^{(0)}(x)$ and $C_{2,G}^{(0)}(x)$ terms are not the only ones that must be subtracted. Still, we double count the corresponding collinear configurations which are a part of the DGLAP equations and manifest themselves via the splitting functions P_{ij} and k_i. Such configurations give rise to terms proportional to $\ln Q^2$ and through DGLAP equations are part of the heavy-quark densities $q_h^\gamma(x,Q^2)$. The same collinear configurations appear in massive heavy-quark Wilson coefficients $C_{2,j}^{h,(n)}$. Therefore, we must subtract the overlapping contributions. In the case of our model, where we neglect the higher order heavy-quark Wilson coefficients, there are only two such terms, same as in the LO case described in [1,2]. They are related to the $\gamma^* + \gamma \to h + \bar{h}$ and $\gamma^* + G \to h + \bar{h}$ processes. We calculate the necessary subtraction terms from the approximated integration of the corresponding parts of the DGLAP equations (6) and (7) over the region (Q_0^2, Q^2) (see [2]). The integration produces the $\ln(Q^2/Q_0^2)\cdot e_h^2(\alpha/2\pi)k_q^{(0)}(x)$ and $\ln(Q^2/Q_0^2)\cdot[\alpha_s(Q^2)/2\pi]\times\int_{\chi_h}^1(dy/y)P_{qG}^{(0)}(x/y)G(y,Q^2)$ terms [20]. These terms multiplied by $2x$ and e_h^2, according to the formula $F_2^\gamma(x,Q^2) = \sum_q x e_i^2(q^\gamma + \bar{q}^\gamma)(x,Q^2)$, must be subtracted from the sum of Eq. (17).

The described summation and subtraction procedure leads to the following formula for the $F_2^\gamma(x,Q^2)$:

$$\begin{aligned}\frac{1}{x}F_2^\gamma(x,Q^2) = \sum_{i=1}^{3} e_i^2\Big\{&(q_i^\gamma+\bar{q}_i^\gamma)(x,Q^2) + e_i^2\frac{\alpha}{2\pi}C_{2,\gamma}^{(0)}(x) + \frac{\alpha_s(Q^2)}{2\pi}\int_x^1\frac{dy}{y}\Big[(q_i^\gamma+\bar{q}_i^\gamma)(y,Q^2)C_{2,q}^{(1)}\Big(\frac{x}{y}\Big)\\ &+G^\gamma(y,Q^2)C_{2,G}^{(1)}\Big(\frac{x}{y}\Big)\Big]\Big\} + \sum_{h(=c,b)}^{2} e_h^2\Big\{(q_h^\gamma+\bar{q}_h^\gamma)(x,Q^2) + e_h^2\frac{\alpha}{2\pi}C_{2,\gamma}^{h,(0)}\Big(x,\frac{Q^2}{m_h^2}\Big)\\ &+\frac{\alpha_s(Q^2)}{2\pi}\Big[\int_x^1\frac{dy}{y}(q_h^\gamma+\bar{q}_h^\gamma)(y,Q^2)C_{2,q}^{(1)}\Big(\frac{x}{y}\Big) + \int_{\chi_h}^1\frac{dy}{y}G^\gamma(y,Q^2)C_{2,G}^{h,(1)}\Big(\frac{x}{y},\frac{Q^2}{m_h^2}\Big)\Big] - \ln\frac{Q^2}{Q_0^2}\cdot 2e_h^2\frac{\alpha}{2\pi}k_q^{(0)}(x)\\ &-\ln\frac{Q^2}{Q_0^2}\cdot 2\frac{\alpha_s(Q^2)}{2\pi}\int_x^1\frac{dy}{y}G^\gamma(y,Q^2)P_{qG}^{(0)}\Big(\frac{x}{y}\Big)\Big\}.\end{aligned} \tag{18}$$

Its graphical representation is given in Fig. 3. If one includes the $O(\alpha_s^2)$ and $O(\alpha\alpha_s)$ heavy-quark contributions, the structure of the subtraction terms becomes more complicated, since one has to subtract terms proportional to $k_q^{(1)}(x)$, $P_{qG}^{(1)}(x)$, and $P_{qq}^{(1)}(x)$. Moreover these functions are divergent at $x = 1$ and therefore their in-

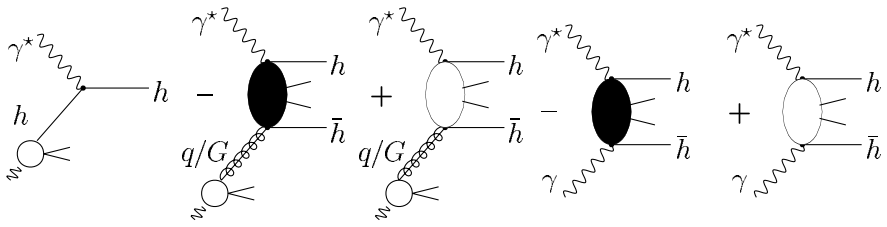

FIG. 3. Graphical representation of the contributions to the CJK NLO model. The first diagram represents the ZVFNS contribution. The third and fifth diagrams show the FFNS resolved-photon and direct-photon contributions, respectively. The second and fourth diagrams are the corresponding subtraction terms.

tegrals lead to numerical instabilities. Solution of that problem is beyond the scope of this work.

D. The $\overline{\text{MS}}$ and DIS$_\gamma$ factorization schemes

The introduction of the heavy-quark contributions to the $F_2^\gamma(x, Q^2)$ forces us to apply a modified DIS$_\gamma$ scheme in the CJK NLO model case. Let us recall that in this model apart from the massless, divergent at $x \to 1$ contribution of light quarks, $C_{2,\gamma}^{(0)}(x)$, the massive, finite $C_{2,\gamma}^{h,(0)}[x, (Q^2/m_h^2)]$ term appears as the analogous heavy-quark contribution. In order to remove the large-x divergence of the $C_{2,\gamma}^{(0)}(x)$ we proceed in the same way as described in the FFNS approach, absorbing that term into the light-quark distribution functions $q_i^\gamma(x, Q^2)$. What about the massive $C_{2,\gamma}^{h,(0)}[x, (Q^2/m_h^2)]$ contribution and the heavy-quark densities? The charm- and beauty-quark distributions in the CJK NLO model appear as a part of the massless ZVFNS scheme. The evolution of all partons is performed through the common set of five-flavor DGLAP evolution equations. Therefore, the subtraction of the $C_{2,\gamma}^{(0)}(x)$ term from Eq. (18) and modification of the k_{q_i} and k_G splitting functions [expressed in Eq. (13)] affect the heavy-quark densities in the same way as they affect the light-quark distributions. Namely, the following redefinition occurs:

$$q_h^{\text{DIS}_\gamma}(x, Q^2) = q_h^{\overline{\text{MS}}}(x, Q^2) + e_h^2 \frac{\alpha}{4\pi} C_{2,\gamma}^{(0),\overline{\text{MS}}}(x),$$

$$C_{2,\gamma}^{h,(0),\text{DIS}_\gamma}\left(x, \frac{Q^2}{m_h^2}\right) = C_{2,\gamma}^{h,(0),\overline{\text{MS}}}\left(x, \frac{Q^2}{m_h^2}\right) + \Delta C_{2,\gamma}^{(0)}(x). \quad (19)$$

As $\Delta C_{2,\gamma}^{(0)}(x) = -C_{2,\gamma}^{(0),\overline{\text{MS}}}(x)$, see Eq. (12), the last equality takes the form

$$C_{2,\gamma}^{h,(0),\text{DIS}_\gamma}\left(x, \frac{Q^2}{m_h^2}\right) = C_{2,\gamma}^{h,(0),\overline{\text{MS}}}\left(x, \frac{Q^2}{m_h^2}\right) - C_{2,\gamma}^{(0),\overline{\text{MS}}}(x). \quad (20)$$

In practice the subtraction of Eq. (20) cannot be performed in such a simple way. Again, the $C_{2,\gamma}^{(0),\overline{\text{MS}}}(x)$ term on the right side would lead to a divergence at large x and the advantage of the DIS$_\gamma$ scheme would be lost. We have to proceed in a different way.

We decide to resolve the above problem by losing part of the information brought by the massive $C_{2,\gamma}^{h,(0),\overline{\text{MS}}}(x)$ contribution. That term calculated in the $m_h^2 \approx 0$ approximation leads to (see the Appendix)

$$C_{2,\gamma}^{h,(0),\overline{\text{MS}}}\left(x, \frac{Q^2}{m_h^2}\right) = C_{2,\gamma}^{(0),\overline{\text{MS}}}(x) + 2k_q^{(0),\overline{\text{MS}}}(x) \ln\frac{Q^2}{m_h^2} + 6\left\{-\beta x(1-x)\frac{4m_h^2}{Q^2} + \left[x(1-3x)\frac{4m_h^2}{Q^2} - x^2\frac{8m_h^4}{Q^4}\right]\ln\frac{1+\beta}{1-\beta}\right\}, \quad (21)$$

where we keep the heavy-quark mass and $\beta = \sqrt{1 - [4m_h^2 x/(1-x)Q^2]}$ wherever it is possible. Let us notice now that the term $\sim k_q^{(0),\overline{\text{MS}}}(x)$ of Eq. (21) differs from the first subtraction term in Eq. (18) only by the constant $\sim \ln(m_h^2/Q_0^2)$. We omit that constant and obtain in the $\overline{\text{MS}}$ scheme:

$$C_{2,\gamma}^{h,(0),\overline{\text{MS}}}\left(x, \frac{Q^2}{m_h^2}\right) - \ln\frac{Q^2}{Q_0^2} \cdot 2k_q^{(0),\overline{\text{MS}}}(x) \approx C_{2,\gamma}^{(0),\overline{\text{MS}}}(x) + 6\left\{-\beta x(1-x)\frac{4m_h^2}{Q^2} + \left[x(1-3x)\frac{4m_h^2}{Q^2} - x^2\frac{8m_h^4}{Q^4}\right]\ln\frac{1+\beta}{1-\beta}\right\}, \quad (22)$$

which according to Eq. (20) leads to the following relation in the DIS$_\gamma$ scheme:

$$\frac{\alpha}{2\pi} e_h^4 C_{2,\gamma}^{h,(0),\text{DIS}_\gamma}\left(x, \frac{Q^2}{m_h^2}\right) - \ln\frac{Q^2}{Q_0^2} \cdot 2e_h^4 \frac{\alpha}{2\pi} k_q^{(0),\overline{\text{MS}}}(x) \approx 3e_h^4 \frac{\alpha}{\pi}\left\{-\beta x(1-x)\frac{4m_h^2}{Q^2} + \left[x(1-3x)\frac{4m_h^2}{Q^2} - x^2\frac{8m_h^4}{Q^4}\right]\ln\frac{1+\beta}{1-\beta}\right\}. \quad (23)$$

In the following we use only the DIS$_\gamma$ factorization scheme and omit the superscript for simplicity.

E. The χ_h variables

Let us recall that VFNS schemes widely utilize an approach in which $q_h^\gamma(x, Q^2) = 0$ for all Q^2 values smaller than m_h^2 and $q_h^\gamma(x, Q^2)$ becomes nonzero for $Q^2 \geq m_h^2$. At each such step the number of active quarks grows by 1. This approach leads to unphysical heavy-quark densities near their production thresholds. The kinematical threshold of the heavy-quark production, and therefore its nonzero density in the photon, is given in DIS$_{e\gamma}$ by the total energy of the $e\gamma^*$ process, W. As discussed in Sec. II, W must be greater than the sum of two masses of the heavy quark in hand, $W > 2m_h$. W and Q^2 are connected, $W^2 = (1-x)Q^2/x$, which is the reason why the ZVFNS condition $Q^2 \geq m_h^2$ for treating the heavy quark h as a parton is too simple.

In the ACOT(χ) scheme used by the CJK NLO model the number of active quarks is five at the whole range of the DGLAP evolution. To ensure that a heavy-quark,

$q_h^\gamma(x, Q^2)$, distribution disappears when $W \to 2m_h$ one introduces a new variable $\chi_h \equiv x(1 + 4m_h^2/Q^2)$ and calculates $q_h^\gamma(\chi_h, Q^2)$ instead of $q_h^\gamma(x, Q^2)$. At threshold, when $W = 2m_h$, we obtain $\chi_h = 1$ and the corresponding heavy-quark density vanishes as desired. The form of the χ_h variables could be chosen differently if only their above threshold behavior was preserved. We chose to apply the same form as appears in the integration of the massive heavy-quark Wilson coefficients with the parton distributions; see also [5]. That way the same variable takes care of the proper vanishing of the h-quark density and of the $\sim \int_{\chi_h}^1 (dy/y) G^\gamma(y, Q^2) C_{2,G}^{h,(1)}[(x/y), (Q^2/m_h^2)]$ contribution to $F_2^\gamma(x, Q^2)$ at the kinematic limit. For the consistency of the approach also in the subtraction $\sim \int_x^1 (dy/y) P_{qG}^{(0)}(x/y) G^\gamma(y, Q^2)$ term we exchange x with χ_h and that way enforce its proper kinematic behavior.

As described in [1,2] the subtraction $\sim k_q^{(0)}(x)$ term does not vanish as $W \to 2m_h$ even when one replaces x with χ_h. In the NLO case we avoid that problem because, as discussed in Sec. IV D, that contribution cancels in the modified DIS_γ factorization scheme.

Unfortunately, a particular heavy-quark contribution appears in the NLO analysis which causes new problems at threshold. The contribution $\sim \int_x^1 (dy/y)(q_h^\gamma + \bar{q}_h^\gamma)(y, Q^2) \times C_{2,q}^{(1)}(x/y)$ from the ZVFNS scheme could be rewritten in two ways, as $\sim \int_{\chi_h}^1 (dy/y)(q_h^\gamma + \bar{q}_h^\gamma)(y, Q^2) \times C_{2,q}^{(1)}(x/y)$ or as $\sim \int_x^1 (dy/y)(q_h^\gamma + \bar{q}_h^\gamma)(\gamma_h, Q^2) C_{2,q}^{(1)}(x/y)$, with γ_h defined analogously to χ_h [$\gamma_h = y(1 + 4m_h^2/Q^2)$]. The first approach leads to numerical instabilities for y values close to x originating from the $[(1 + x^2)/(1 - x)] \ln[(1 - x)/x]$ term in $C_{2,q}^{(1)}(\frac{x}{y})$. The second form cannot be adopted for technical reasons in Mellin space. Therefore, we use the unmodified formula of Eq. (18). Finally, to avoid the nonzero heavy-quark contributions in the kinematically forbidden (x, Q^2) region we impose by hand the following constraint: $\int_x^1 (dy/y) \times (q_h + \bar{q}_h)(y, Q^2) C_{2,q}^{(1)}(x/y) = 0$ for $\chi_h > 1$. Obviously, the same reasoning would apply to higher order $C_{2,q}^{(j)}$ coefficients neglected in the CJK NLO model.

F. Formula for F_2^γ

Summing the light- and heavy-quark contributions, converting them into the DIS_γ factorization scheme and finally introducing the χ_h variables we obtain the final formula of the $F_2^\gamma(x, Q^2)$ in the CJK NLO model:

$$\begin{aligned}\frac{1}{x} F_2^\gamma(x, Q^2) = {} & \sum_{i=1}^{3} e_i^2 \left\{ (q_i^\gamma + \bar{q}_i^\gamma)(x, Q^2) + \frac{\alpha_s(Q^2)}{2\pi} \int_x^1 \frac{dy}{y} \left[(q_i^\gamma + \bar{q}_i^\gamma)(y, Q^2) C_{2,q}^{(1)}\left(\frac{x}{y}\right) + G^\gamma(y, Q^2) C_{2,G}^{(1)}\left(\frac{x}{y}\right) \right] \right\} \\ & + \sum_{h=1}^{2} e_h^2 \left((q_h^\gamma + \bar{q}_h^\gamma)(\chi_h, Q^2) + \frac{\alpha_s(Q^2)}{2\pi} \left[\int_x^1 \frac{dy}{y} (q_h^\gamma + \bar{q}_h^\gamma)(y, Q^2) C_{2,q}^{(1)}\left(\frac{x}{y}\right) + \int_{\chi_h}^1 \frac{dy}{y} G^\gamma(y, Q^2) C_{2,G}^{h,(1)}\left(\frac{x}{y}, \frac{Q^2}{m_h^2}\right) \right.\right. \\ & \left.\left. - \ln\frac{Q^2}{Q_0^2} \times 2 \int_{\chi_h}^1 \frac{dy}{y} G^\gamma(y, Q^2) P_{qG}^{(0)}\left(\frac{\chi_h}{y}\right) \right] + 3 e_h^2 \frac{\alpha}{\pi} \left\{ -\beta x(1 - x) \frac{4m_h^2}{Q^2} + \left[x(1 - 3x) \frac{4m_h^2}{Q^2} - x^2 \frac{8m_h^4}{Q^4} \right] \ln\frac{1 + \beta}{1 - \beta} \right\} \right). \end{aligned} \tag{24}$$

To prevent the unphysical situation, in which the ZVFNS scheme contribution to $F_2^\gamma(x, Q^2)$ is negative, or in other words in which the total $F_2^\gamma(x, Q^2)$ is smaller than the FFNS scheme contribution, as in [1–3], separately for each heavy quark, we impose an additional positivity condition, here in the form:

$$\begin{aligned}(q_h^\gamma + \bar{q}_h^\gamma)(\chi_h, Q^2) + \frac{\alpha_s}{2\pi} \left[\int_x^1 \frac{dy}{y} (q_h^\gamma + \bar{q}_h^\gamma)(y, Q^2) \times \right. \\ \left. C_{2,q}^{(1)}\left(\frac{x}{y}\right) - \ln\frac{Q^2}{Q_0^2} \cdot 2 \int_{\chi_h}^1 \frac{dy}{y} G^\gamma(y, Q^2) P_{qG}^{(0)}\left(\frac{\chi_h}{y}\right) \right] \geq 0. \end{aligned} \tag{25}$$

V. GLOBAL FITS—SOLVING THE DGLAP EVOLUTION

In this section the technical details of the solution of the DGLAP evolution equations are described.

A. Mellin moments

The DGLAP evolution equations (6) and (7) as well as the structure-function formulas (14) and (24) are very much simplified if they are transformed into the Mellin-moments space. The nth moment, where n is a complex number, for any function f, generally depending on x and Q^2 is defined by $f^n(Q^2) = \int_0^1 x^{n-1} f(x, Q^2) dx$. We apply this definition to the parton distributions, splitting functions and the light-quark Wilson coefficients $C_{2,i}^{(k)}(x)$. Their convolution integrals in the (x, Q^2) space transform into multiplication of the corresponding moments in the Mellin space. This simple correspondence does not hold in the case of the convolutions with the heavy-quark Wilson coefficient $C_{2,G}^{h,(1)}[x, (Q^2/m_h^2)]$ and the $P_{qG}^{(0)}(x)$ splitting function because of the integration limit χ_h. Therefore those integrations must be performed in the (x, Q^2) space. All results calculated in the Mellin space are transformed through the inverse Mellin transformation to obtain their values in the (x, Q^2) space.

B. Nonsinglet and singlet parton densities

In the photon case we define the singlet (Σ^γ) and nonsinglet ($f^\gamma_{\mathrm{NS}(N_f)}$) quark distributions as

$$f^\gamma_{\mathrm{NS}(N_f)}(x,Q^2)=\sum_{i=1}^{N_f}(e_i^2-\langle e^2\rangle)[q_i^\gamma(x,Q^2)+\bar q_i^\gamma(x,Q^2)],$$
$$\Sigma^\gamma(x,Q^2)=\sum_{i=1}^{N_f}[q_i^\gamma(x,Q^2)+\bar q_i^\gamma(x,Q^2)], \tag{26}$$

with

$$\langle e^k\rangle=N_f^{-1}\sum_{i=1}^{N_f}e_i^k. \tag{27}$$

For the singlet density we sum over all quark flavors appearing in the evolution, the active quarks, $N_f=5$. Although in the CJK model $N_f=5$, for the nonsinglet case it is necessary to calculate all $q^\gamma_{\mathrm{NS}(3)}$, $q^\gamma_{\mathrm{NS}(4)}$, and $q^\gamma_{\mathrm{NS}(5)}$ (x,Q^2) to obtain all six parton distributions; see [1].

The evolution of the nonsinglet distributions is governed by the simplified DGLAP equation. In the Mellin-moments space it reads

$$\frac{df^{\gamma,n}_{\mathrm{NS}(N_f)}(Q^2)}{d\ln Q^2}=\frac{\alpha}{2\pi}k^n_{\mathrm{NS}(N_f)}+\frac{\alpha_s(Q^2)}{2\pi}P^{\mathrm{NS},n}_{qq}f^{\gamma,n}_{\mathrm{NS}(N_f)}(Q^2). \tag{28}$$

The singlet distribution evolution is coupled with the evolution of the gluon density

$$\frac{d\Sigma^{\gamma,n}(Q^2)}{d\ln Q^2}=\frac{\alpha}{2\pi}k^n_\Sigma+\frac{\alpha_s(Q^2)}{2\pi}[P^n_{\Sigma\Sigma}\Sigma^{\gamma,n}(Q^2)+P^n_{\Sigma G}G^{\gamma,n}(Q^2)], \tag{29}$$

$$\frac{dG^{\gamma,n}(Q^2)}{d\ln Q^2}=\frac{\alpha}{2\pi}k^n_G+\frac{\alpha_s(Q^2)}{2\pi}[P^n_{G\Sigma}\Sigma^{\gamma,n}(Q^2)+P^n_{GG}G^{\gamma,n}(Q^2)]. \tag{30}$$

Therefore, one has to solve the matrix equation

$$\frac{d\vec f^{\,\gamma,n}_{\mathrm{S}}(Q^2)}{d\ln Q^2}=\frac{\alpha}{2\pi}\vec k^n_{\mathrm{S}}+\frac{\alpha_s}{2\pi}\hat P^{\mathrm{S},n}\vec f^{\,\gamma,n}_{\mathrm{S}}(Q^2), \tag{31}$$

with

$$\vec f^{\,\gamma,n}_{\mathrm{S}}=\begin{bmatrix}\Sigma^{\gamma,n}\\ G^{\gamma,n}\end{bmatrix},\qquad \vec k^n_{\mathrm{S}}=\begin{bmatrix}k^n_\Sigma\\ k^n_G\end{bmatrix},$$
$$\hat P^{\mathrm{S},n}=\begin{bmatrix}P^n_{\Sigma\Sigma} & P^n_{\Sigma G}\\ P^n_{G\Sigma} & P^n_{GG}\end{bmatrix}. \tag{32}$$

The new pointlike splitting functions are defined as

$$k_{\mathrm{NS}(N_f)}(x)=2N_f(\langle e^4\rangle-\langle e^2\rangle^2)\left[k_q^{(0)}+\frac{\alpha_s(Q^2)}{2\pi}k_q^{(1)}\right](x),$$
$$k_\Sigma(x)=2N_f\langle e^2\rangle\left[k_q^{(0)}+\frac{\alpha_s(Q^2)}{2\pi}k_q^{(1)}\right](x). \tag{33}$$

The formulas for the above splitting functions $P_{ij}(x,Q^2)$ can be found for instance in [17]. Their Mellin moments were calculated in [21].

C. Point- and hadronlike parts

The solution to the DGLAP equations can be divided into the so-called pointlike (pl) part, related to a special solution of the full inhomogenous equations and hadronlike (had) part, being a general solution of the homogenous equations. Their sum gives the parton density in the photon, so we have

$$f^{\gamma,n}_{\mathrm{NS}(N_f)}(Q^2)=f^{\gamma,n}_{\mathrm{NS}(N_f),\mathrm{had}}(Q^2)+f^{\gamma,n}_{\mathrm{NS}(N_f),\mathrm{pl}}(Q^2), \tag{34}$$

$$\vec f^{\,\gamma,n}_{\mathrm{S}}(Q^2)=\vec f^{\,\gamma,n}_{\mathrm{S,had}}(Q^2)+\vec f^{\,\gamma,n}_{\mathrm{S,pl}}(Q^2). \tag{35}$$

The nonsinglet hadronlike solution is given as

$$f^{\gamma,n}_{\mathrm{NS}(N_f),\mathrm{had}}(Q^2)=L^{-2P^{(0),n}_{qq}/\beta_0}\left\{1-\frac{\alpha_s(Q^2)-\alpha_s(Q_0^2)}{\pi\beta_0}\hat R\right\}f^{\gamma,n}_{\mathrm{NS}(N_f),\mathrm{had}}(Q_0^2) \tag{36}$$

and the nonsinglet pointlike solution is

$$f^{\gamma,n}_{\mathrm{NS}(N_f),\mathrm{pl}}(Q^2)=\frac{4\pi}{\alpha_s(Q^2)}[1-L^{1-2P^{(0)n}_{qq}/\beta_0}]a^n+[1-L^{-2P^{(0)n}_{qq}/\beta_0}]b^n, \tag{37}$$

with

$$a^n=\frac{\alpha}{2\pi\beta_0}\frac{k^{(0)n}_{\mathrm{NS}}}{1-2P^{(0)n}_{qq}/\beta_0},$$
$$b^n=-\frac{1}{P^{(0)n}_{qq}}\left[2\hat R a^n+\frac{\alpha}{2\pi}\hat K\right] \tag{38}$$

and

$$L=\frac{\alpha_s(Q^2)}{\alpha_s(Q_0^2)},\qquad \hat R=P^{(1),n}_{\mathrm{NS}}-\frac{\beta_1}{2\beta_0}P^{(0),n}_{qq},$$
$$\hat K=k^{(1),n}_{\mathrm{NS}}-\frac{\beta_1}{2\beta_0}k^{(0),n}_{\mathrm{NS}}. \tag{39}$$

Here β_0 and β_1 are the coefficients of the running strong coupling, α_s, which we discuss in detail in Sec. V E.

The singlet point- and hadronlike solutions have the same form but are more complicated than the corresponding nonsinglet solutions. All formulas can be found for instance in [19].

D. Input parton densities: VMD

The hadronlike parts of the singlet and nonsinglet densities, denoted in this section as $f_{\rm had}$, need input distributions. For this purpose we utilize the vector meson dominance (VMD) model [22], where

$$f^{\gamma}_{\rm had}(x, Q_0^2) = \sum_V \frac{4\pi\alpha}{\hat{f}_V^2} f^V(x, Q_0^2), \tag{40}$$

with the sum running over all light vector mesons (V) into which the photon can fluctuate. The parameters $\hat{f}_V^2$ can be extracted from the experimental data on $\Gamma(V \to e^+e^-)$ width. In practice we take into account the ρ^0 meson while the contributions from the other mesons are accounted for via a parameter κ

$$f^{\gamma}_{\rm had}(x, Q_0^2) = \kappa \frac{4\pi\alpha}{\hat{f}_\rho^2} f^{\rho}(x, Q_0^2), \tag{41}$$

which is left as a free parameter in the fits.

We use the input densities of the ρ^0 meson at low Q_0^2 in the form of valencelike distributions both for the (light) quark (v^ρ) and gluon (G^ρ) densities. All sea-quark distributions (denoted by ζ^ρ) are neglected at the input scale. At this scale, the densities v^ρ, G^ρ, and ζ^ρ are related, according to Eq. (41) to the corresponding densities for a photon, see below.

The v^ρ density is given by

$$v^\rho(x, Q_0^2) = \tfrac{1}{4}(u^{\rho^+} + \bar{u}^{\rho^-} + d^{\rho^-} + \bar{d}^{\rho^+})(x, Q_0^2), \tag{42}$$

where from the isospin symmetry

$$u^{\rho^+}(x, Q_0^2) = \bar{u}^{\rho^-}(x, Q_0^2) = d^{\rho^-}(x, Q_0^2) = \bar{d}^{\rho^+}(x, Q_0^2). \tag{43}$$

Note that all the densities in Eq. (42) are normalized to 1, e.g., $\int_0^1 u^{\rho^+} dx = 1$.

Two constraints should hold for the $v^\rho(x, Q_0^2)$ density; the first one is related to the number of valence quarks in the ρ^0 meson,

$$\int_0^1 2v^\rho(x, Q_0^2) dx = 2, \tag{44}$$

and the second constraint represents the energy-momentum sum rule:

$$\int_0^1 x[2v^\rho(x, Q_0^2) + G^\rho(x, Q_0^2)] dx = 1. \tag{45}$$

We parametrize the input densities as follows:

$$\begin{aligned} &x\zeta^\rho(x, Q_0^2) = 0, \qquad xv^\rho(x, Q_0^2) = N_v x^\alpha (1-x)^\beta, \\ &xG^\rho(x, Q_0^2) = \tilde{N}_G x v^\rho(x, Q_0^2) = N_G x^\alpha (1-x)^\beta, \end{aligned} \tag{46}$$

where $N_G = \tilde{N}_G N_v$. Like in the LO analysis, [1–3], the input gluon distribution is proportional to the valence one and both have the valencelike form. One should treat this as a simple ansatz. A similar form has been used also in the most recent NLO analysis [12]; see also discussion below. Further, we impose two constraints given by Eqs. (44) and (45) in both types of models: $\rm FFNS_{CJK}$ and CJK NLO. These constraints allow us to express the normalization factors N_v and N_G as functions of α, β, and κ. This leaves these three parameters as the only free parameters to be fixed in the fits to the F_2^γ experimental data.

E. α_s running and values of $\Lambda^{(N_q)}$

We distinguish between the number of active quarks in the photon, N_f, and the number of quarks contributing to the running of α_s, which we denote by N_q, [2]. The N_f depends only on the choice of the type of the model: once we decide to use the $\rm FFNS_{CJK}$ or CJK NLO approach, then $N_f = 3$ or 5, respectively, through the whole Q^2 range of evolution. On the contrary N_q depends on the Q^2 value. It is equal to 3 when $Q^2 < m_c^2$ and increases by one unit whenever Q^2 reaches a heavy-quark threshold, i.e., when $Q^2 = m_h^2$.

The running of the strong coupling constant in NLO is given then by the well-known formula:

$$\frac{\alpha_s^{(N_q)}(Q^2)}{4\pi} = \frac{1}{\beta_0 \ln(Q^2/\Lambda^{(N_q)^2})} - \frac{\beta_1}{\beta_0^3} \frac{\ln\ln(Q^2/\Lambda^{(N_q)^2})}{(\Lambda^{(N_q)^2})^2}, \tag{47}$$

with

$$\beta_0 = 11 - \frac{2}{3}N_q, \qquad \beta_1 = 102 - \frac{38}{3}N_q. \tag{48}$$

For $N_q = 4$ we take the QCD scale $\Lambda^{(4)}$ equal to 280 MeV [23]. In order to ensure the continuity of the strong coupling constant at the heavy-quark thresholds the condition $\alpha_s^{(N_q)}(m_h^2) = \alpha_s^{(N_q+1)}(m_h^2)$ is imposed. We calculate values of the remaining $\Lambda^{(N_q)}$ constants according to the above condition, using the relation between constants $\Lambda^{(N_q)}$ and $\Lambda^{(N_q+1)}$ given in [24]. That way we obtain $\Lambda^{(3)} = 0.323$ MeV and $\Lambda^{(5)} = 0.200$ MeV.

The parton evolution equations depend on N_q through their dependence on $\alpha_s(Q^2)$ and independently β_0 and β_1; see Eqs. (36) and (37). Therefore, because of the implicit introduction of the heavy-quark thresholds into the α_s running we must proceed in three steps to perform the DGLAP evolution. In the first step, describing the evolution from the input scale Q_0 to the charm-quark mass m_c, the hadronic input $q^\gamma_{\rm had}(x, Q_0^2)$ is taken from the VMD model. In the second step we evolve the parton distributions from m_c to the beauty-quark mass, m_b. Then, a new hadronic input is given by the sum of the already evolved hadronic and pointlike contributions. The pointlike distribution at $Q^2 = m_c^2$ becomes zero again. The same is repeated for $Q^2 > m_b^2$.

VI. GLOBAL FITS—RESULTS

We have performed a series of fits to the $F_2^\gamma(x, Q^2)$ data [25–38]. All together 192 data points were used, including the recent results of the ALEPH Collaboration [36], which replaced the old preliminary data [39], as well as recent preliminary results of the DELPHI Collaboration [33] replacing the old preliminary data [40]. In that case only the LEP1 data were applied because no final results for the LEP2 data are given in a form useful for our global fits [41] in [33]. Our fits based on the least square principle (minimum of χ^2) were done using MINUIT [45]. Systematic and statistical errors of data points were added in quadrature.

First, we made two test fits in which, following the analysis of the Glück, Reya, and Schienbein (GRS) group, [10], we assumed the input scale value $Q_0^2 = 0.4$ GeV^2. The results of both fits are presented in Table III. The first two columns show the quality of the fits, i.e., the total χ^2 for 192 points and the χ^2 per degree of freedom. The fitted values for parameters α, β, and κ are presented in the middle of the table with the symmetric parabolic errors obtained from MIGRAD requiring $\Delta\chi^2 = 1$ [46]. In addition, the values for N_v and $\tilde{N}_g$ obtained from these parameters, using the constraints (44) and (45), are given in the last two columns. As can be seen the fits give high χ^2 per degree of freedom. Further, the relatively small κ value indicates, respectively, a small contribution of heavier mesons which is compensated by a very high, especially in the case of the CJK NLO model, valence-quark input ($N_v = 9.26$).

In order to obtain better agreement with the data two other fits were performed, in which Q_0^2 was treated at first as a free parameter. For both models we obtained very similar Q_0^2 values: $Q_0^2 \approx 0.765$ GeV^2. Therefore in our final CJK and FFNS$_{\rm CJK}$ NLO fits we fixed the input scale as $Q_0^2 = 0.765$ GeV^2. This value agrees with the $Q_0 = 0.85 \pm 0.09$ GeV obtained in the recent NLO fit presented in [12], where contrary to our analyses the input gluon density is neglected while the sea input is present. The results of both CJK and FFNS$_{\rm CJK}$1 NLO fits are presented in Table IV. The errors shown in the table were obtained from MINOS requiring $\Delta\chi^2 = 1$.

As expected, estimation of the Q_0^2 value through the test fits allowed us to find sets of parameters which give better agreement of both models with the data. We use these sets as the final results of our analysis. Comparison of the $\chi^2/_{\rm d.o.f.}$ values obtained in the test and final fits shows the $\sim$0.40 and $\sim$0.30 improvement in the FFNS$_{\rm CJK}$1 and CJK NLO models, respectively. Further, in both cases we observe an increase of the κ parameter with the simultaneous decrease of α, β, and N_v. That change can be explained by the fact that in higher Q^2 valence distribution broadens (change of α, β) but at the same time the constraint (44) maintains its integral constant. Finally, the $\tilde{N}_G$ parameter grows at higher Q_0^2 because the gluon contribution to the photon structure increases with the increasing Q^2.

The choices of the $F_2^\gamma(x, Q^2)$ distributions predicted by the test and final fits are presented in Figs. 4 and 5 for the FFNS$_{\rm CJK}$1 and CJK NLO models, respectively. As the main difference we observe faster growth of the F_2^γ function at small x in the case of the test fits with $Q_0^2 = 0.4$ GeV^2, especially at small Q^2. The medium- and high-x predictions for the photon structure function are similar apart from the low Q^2 region.

Moreover, we see that unlike in the LO case (see [1,2]), and in the case of the test fits with $Q_0^2 = 0.4$ GeV^2, the obtained χ^2 per degree of freedom is better in the standard type FFNS model than in the CJK model. The origin of the relatively high $\chi^2/_{\rm d.o.f.}$ in both fits comparing to much lower $\chi^2 \approx 0.9$ obtained in [12] is the same as in the LO case, discussed in detail in [3]. Namely, the exclusion of the CELLO [25] and recent DELPHI [33] data from the fits leads to much better agreement among fits and the data.

TABLE III. The χ^2 and parameters of the test fits for 192 data points for FFNS$_{\rm CJK}$1 NLO and CJK NLO models with assumed $Q_0^2 = 0.4$ GeV^2. The α, β, and κ symmetric parabolic errors obtained from MIGRAD requiring $\Delta\chi^2 = 1$.

NLO models	χ^2	$\chi^2/_{\rm d.o.f.}$	κ	α	β	N_v	$\tilde{N}_G$
FFNS$_{\rm CJK}$1	318.0	1.68	1.40 ± 0.06	1.15 ± 0.16	1.24 ± 0.42	2.80	0.949
CJK	299.9	1.51	1.40 ± 0.05	1.38 ± 0.18	3.40 ± 0.77	9.26	2.19

TABLE IV. The χ^2 and parameters of the final fits for 192 data points for FFNS$_{\rm CJK}$1 NLO and CJK NLO models with assumed $Q_0^2 = 0.765$ GeV^2. The α, β, and κ errors obtained from MINOS requiring $\Delta\chi^2 = 1$.

NLO models	χ^2	$\chi^2/_{\rm d.o.f.}$	κ	α	β	N_v	$\tilde{N}_G$
FFNS$_{\rm CJK}$1	243.3	1.29	$2.288^{+0.108}_{-0.096}$	$0.502^{+0.071}_{-0.066}$	$0.690^{+0.282}_{-0.252}$	0.685	2.369
CJK	256.8	1.37	$2.662^{+0.108}_{-0.099}$	$0.496^{+0.063}_{-0.057}$	$1.013^{+0.284}_{-0.255}$	0.745	3.056

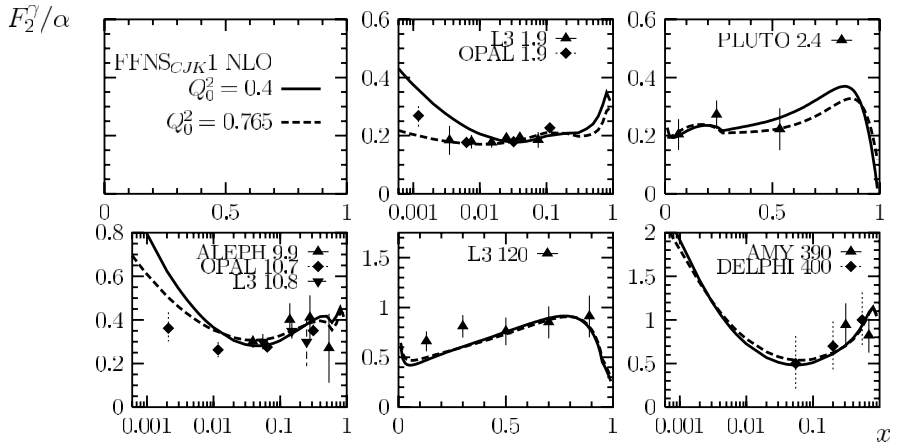

FIG. 4. Predictions for the $F_2^\gamma(x, Q^2)/\alpha$ for the FFNS$_{\rm CJK}$1 NLO model obtained by the main fit with $Q_0^2 = 0.765$ GeV^2 and by the test fit with $Q_0^2 = 0.4$ GeV^2.

Further, we performed test fits with a modified set of the input densities (46). Namely, we used the input gluon distribution independent of the valence one

$$x\zeta^\rho(x, Q_0^2) = 0, \qquad x\upsilon^\rho(x, Q_0^2) = N_\upsilon x^\alpha (1-x)^\beta, \qquad xG^\rho(x, Q_0^2) = N_G x^{\alpha_G}(1-x)^{\beta_G}. \tag{49}$$

Fits gave very high values of the α_G and β_G parameters, around 14 and 16, respectively, leading to fast oscillations of the input gluon densities and all parton densities at low Q^2. The N_G parameter calculated using constraint (45) is of the order 10^9. Moreover, the α_G and β_G values have very high uncertainties and therefore it is hard to obtain the final convergence of the fits. Taking all this and the fact that the $\chi^2/_{\rm d.o.f.}$ values obtained in the test fits are slightly higher than the ones presented above, we conclude that the choice of the simple form of the input distributions of Eqs. (46) is very reasonable even at $Q_0^2 \approx 0.8$ GeV^2.

A. Comparison of the CJK and FFNS$_{\rm CJK}$ NLO fits with F_2^γ data and other NLO parametrizations

Figures 6–9 show a comparison of the CJK and FFNS$_{\rm CJK}$1 NLO fits to $F_2^\gamma(x, Q^2)$ with the experimental data as a function of x, for different values of Q^2. Also a comparison with the GRS NLO [10] and Aurenche, Fontannaz, Guillet (AFG) NLO [47] parametrizations is shown. (If a few values of Q^2 are displayed in a panel, the average of the smallest and biggest one was taken in the computation.) As can be seen in Figs. 6 and 7, both CJK and FFNS$_{\rm CJK}$1 NLO models predict a much steeper behavior of the $F_2^\gamma(x, Q^2)$ at small x with respect to other parametrizations. In the region of medium and high x, the behavior of the $F_2^\gamma(x, Q^2)$ obtained from the FFNS$_{\rm CJK}$1 and CJK NLO fits is similar to the one computed with the GRS NLO parametrization while it is very different from the AFG parametrization prediction; see Figs. 8 and 9. Below the charm-quark threshold the CJK model gives the highest F_2^γ and the GRS NLO parametrization the lowest F_2^γ of the three similar predictions while above the

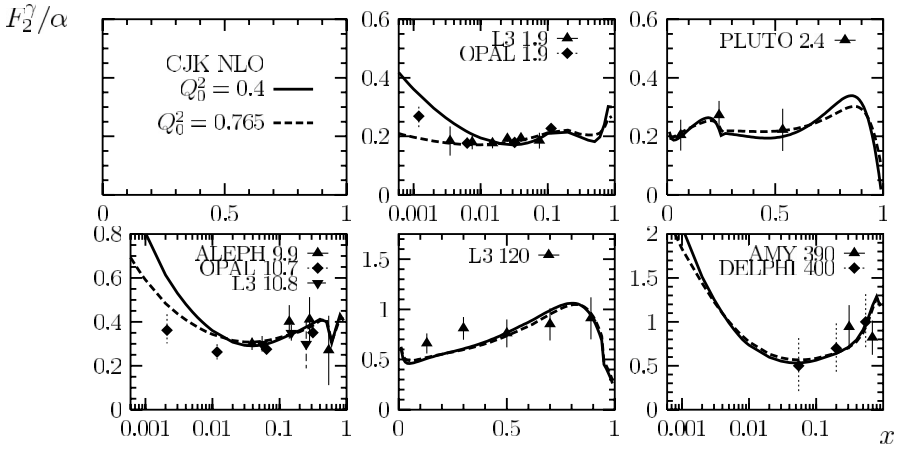

FIG. 5. The same as in Fig. 4 for the CJK NLO model.

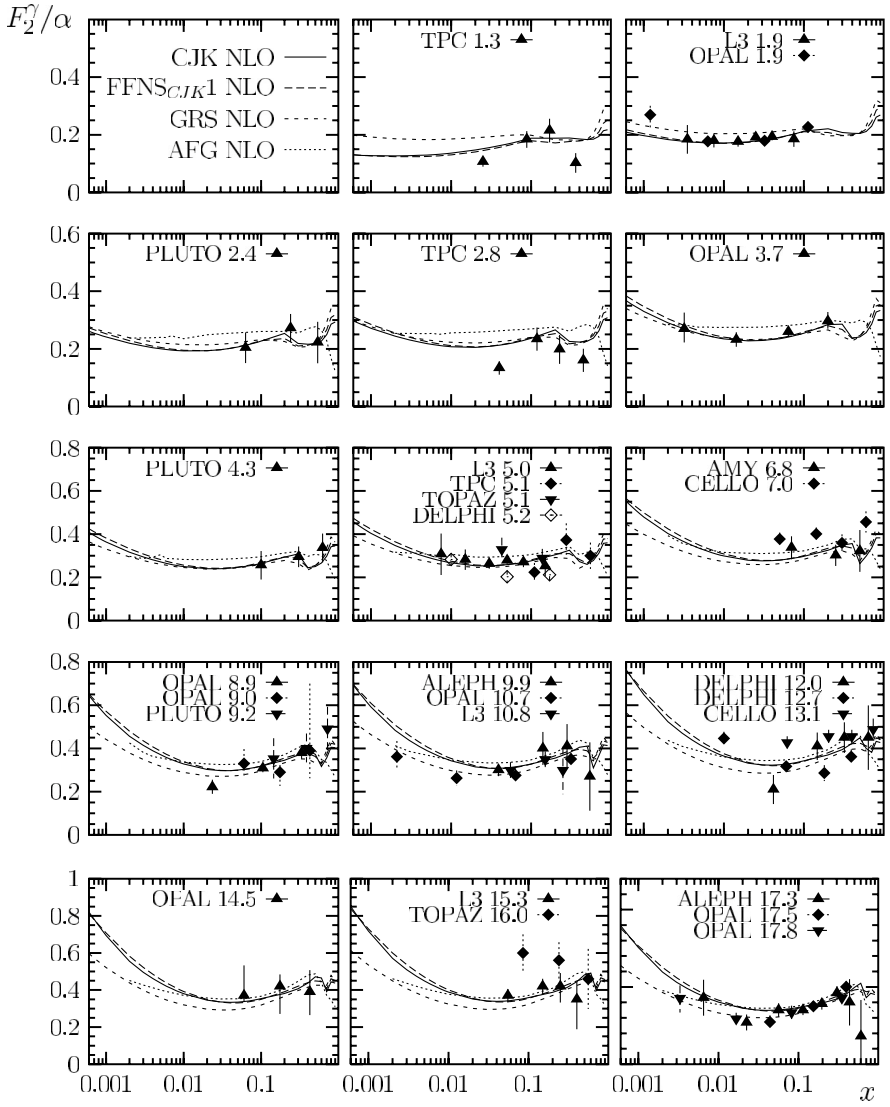

FIG. 6. Predictions for the $F_2^\gamma(x, Q^2)/\alpha$ for the CJK NLO and FFNS$_{\rm CJK}$ NLO models and GRS NLO [10] and AFG NLO [47] compared with the experimental data [25–38], for small and medium Q^2 as a function of x (logarithmic scale). If a few values of Q^2 are displayed in the panel, the average of the smallest and biggest Q^2 was taken in the computation.

threshold that order is inverted. Finally, at high Q^2 and high x the F_2^γ computed in the FFNS$_{\rm CJK}$1 NLO model and GRS NLO parametrization become undistinguishable while the CJK NLO prediction is visibly larger.

Next, in Figs. 10 and 11 we compare the CJK and FFNS$_{\rm CJK}$1 NLO fits with the corresponding CJK and FFNS$_{\rm CJK}$2 LO fits presented in [2]. Figure 10 shows very small differences; only in the low x region the FFNS$_{\rm CJK}$1 NLO model gives greater values than other models and parametrizations. On the other hand, as can be seen in Fig. 11, the NLO models predict higher F_2^γ than the LO ones at the x region right below the charm-quark threshold. Moreover the NLO predictions vanish more rapidly at $x \to 1$.

Apart from the direct comparison with the photon structure-function data, we perform another comparison, this time with LEP data that were not used directly in our analysis. Figures 12 and 13 present the predictions for $F_2^\gamma(x, Q^2)$, averaged over various x regions, compared with the recent OPAL data [38]. For comparison, the results from the GRS and AFG NLO parametrizations are shown as well. In Fig. 12 we observe that in the medium-x range, $0.1 < x < 0.6$, all models give expectations of the same shape, all in fairly good agreement with the experimental data. Still, in small Q^2 the F_2^γ computed with the AFG NLO parametrization is above the others, and starting at approximately $Q^2 = 3$ GeV^2 the predictions of the GRS NLO parametrization are lower than the other three. In the x ranges presented in Fig. 13 we also notice many differences among the averaged $F_2^\gamma(x, Q^2)$ predictions computed in various models. The only exceptions give the FFNS$_{\rm CJK}$1 NLO and the GRS NLO predic-

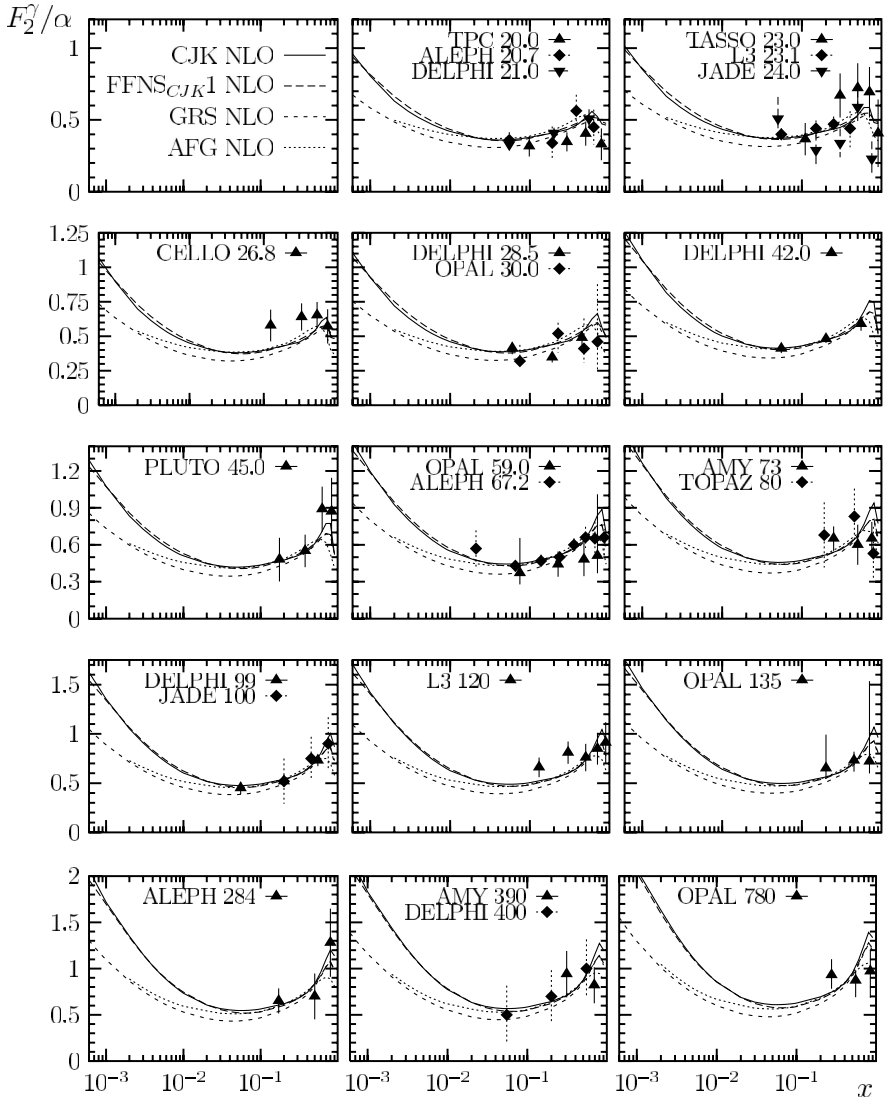

FIG. 7. The same as in Fig. 6, for $Q^2 \geq 20$ GeV^2.

tions which are very close to each other in the whole Q^2 range and in all, apart from the lowest, x ranges examined. Let us now name all the dissimilarities observed in Fig. 13. First, the $F_2^\gamma(Q^2)$ predicted by the CJK NLO model shows a clear change of the behavior in the high Q^2 and high-x range where we observe its larger increase than predicted by the other models. Second, the expectations of the AFG parametrization in the same regions (also for small Q^2) lie much below the other results. Finally, the GRS NLO parametrization predicts slightly lower $F_2^\gamma(Q^2)$ values than the remaining models.

B. Parton densities

In this section we present the parton densities obtained from the CJK and FFNS$_{\rm CJK}$1 NLO fits and compare them with the corresponding distributions of the GRV [9], GRS, and AFG NLO parametrizations. First, we present all parton densities at $Q^2 = 10$ GeV^2 (Fig. 14). The biggest difference between our CJK NLO model and others is observed, as expected, for the heavy-quark distributions. Unlike for the GRV and AFG NLO parametrizations (there is no beauty-quark density in the AFG NLO parametrization), our $c^\gamma(x, Q^2)$ and $b^\gamma(x, Q^2)$ densities vanish not at $x = 1$ but, as it should be, at the kinematical threshold. Moreover, we notice a huge difference between the beauty-quark distributions computed in the CJK NLO and GRV NLO models. Indeed, the latter predicts a b-quark distribution very similar to the c-quark one, while much smaller values for $b^\gamma(x, Q^2)$ are expected in the CJK NLO model. In Fig. 15, where the charm-quark distributions are presented for various Q^2 values, apart from different threshold behavior we observe that CJK $c^\gamma(x, Q^2)$ distribution is the largest of all down to very small-x values where the GRV density becomes larger (the x value at which this occurs depends on Q^2, being larger

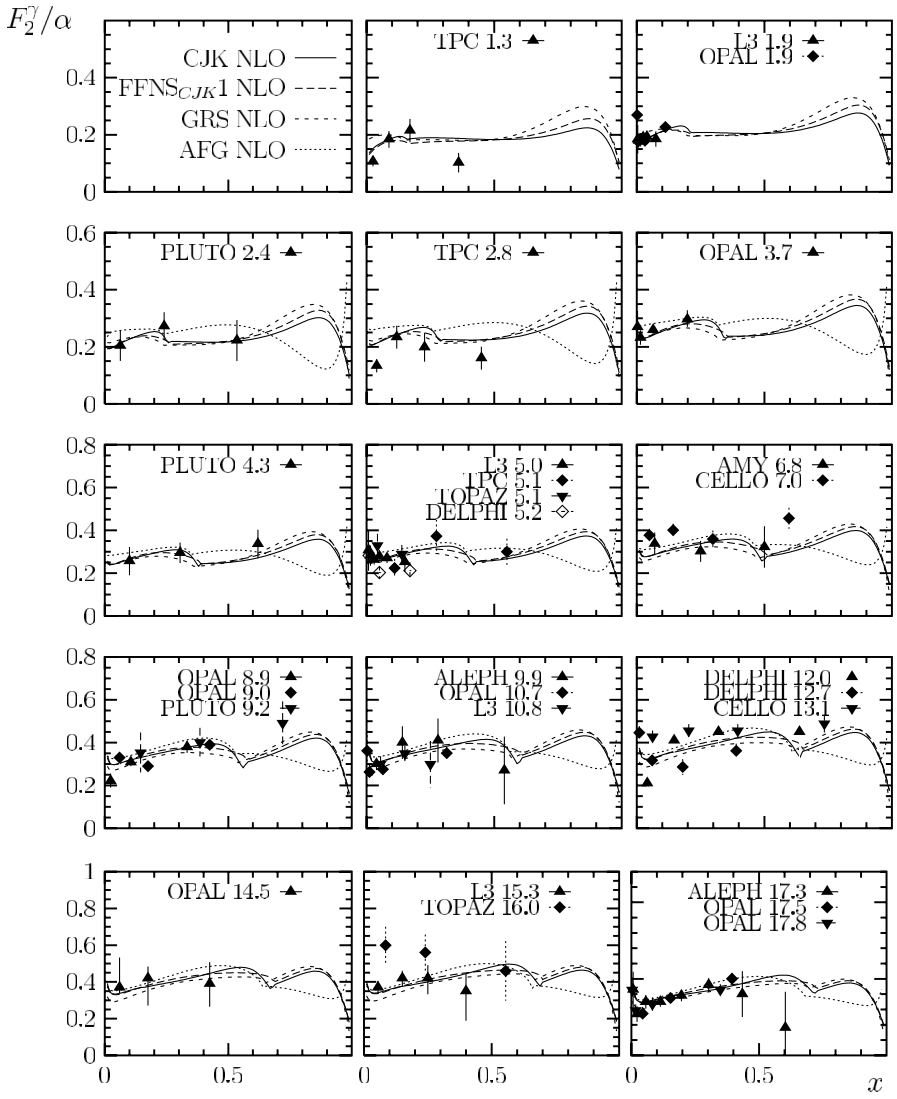

FIG. 8. The same as in Fig. 6 for a linear scale in x.

for larger Q^2). The light-quark and gluon densities calculated in our models and the GRV and GRS NLO parametrizations generally have the same shapes but their values differ. Main differences are observed in the up-, down-quark, and gluon distributions. The u^γ densities computed in both our models are lower than in other parametrizations at high x. In Fig. 16 we see differences among predictions of all models at very low x. Still we do not find a general pattern of those distinctions. In the case of the gluon distribution, see Figs. 14 and 17, we observe that at all Q^2 regions the CJK model gives the largest predictions. At high Q^2, $G^\gamma(x, Q^2)$ calculated in the FFNS$_{\rm CJK}$1 NLO model and in GRV NLO parametrization become similar. The GRS and AFG NLO predictions lie below all other lines in the whole x and Q^2 range.

Further, we compare our CJK and FFNS$_{\rm CJK}$1 NLO parton distributions with the corresponding CJK and FFNS$_{\rm CJK}$2 LO ones. As can be seen in Fig. 18, for $Q^2 = 10$ GeV^2, the NLO models predict higher up- and down-quark densities in the medium-x region and steeper increase when decreasing x of the gluon distribution. The growth of $G^\gamma(x, Q^2)$ at low x is especially fast in the CJK NLO model case while the FFNS$_{\rm CJK}$1 NLO model prediction tends to fuse with the LO ones. Moreover, all NLO quark densities vanish more rapidly at $x \to 1$ than the LO quark densities.

C. Comparison with $F_{2,c}^\gamma$

In Fig. 19 we present the CJK NLO predictions for the $F_{2,c}^\gamma$. For $Q^2 = 5$, 20, 100, and 1000 GeV^2 we compare the individual contributions included in the model. Analogously to the LO case, see [1,2], we introduce the following notation:

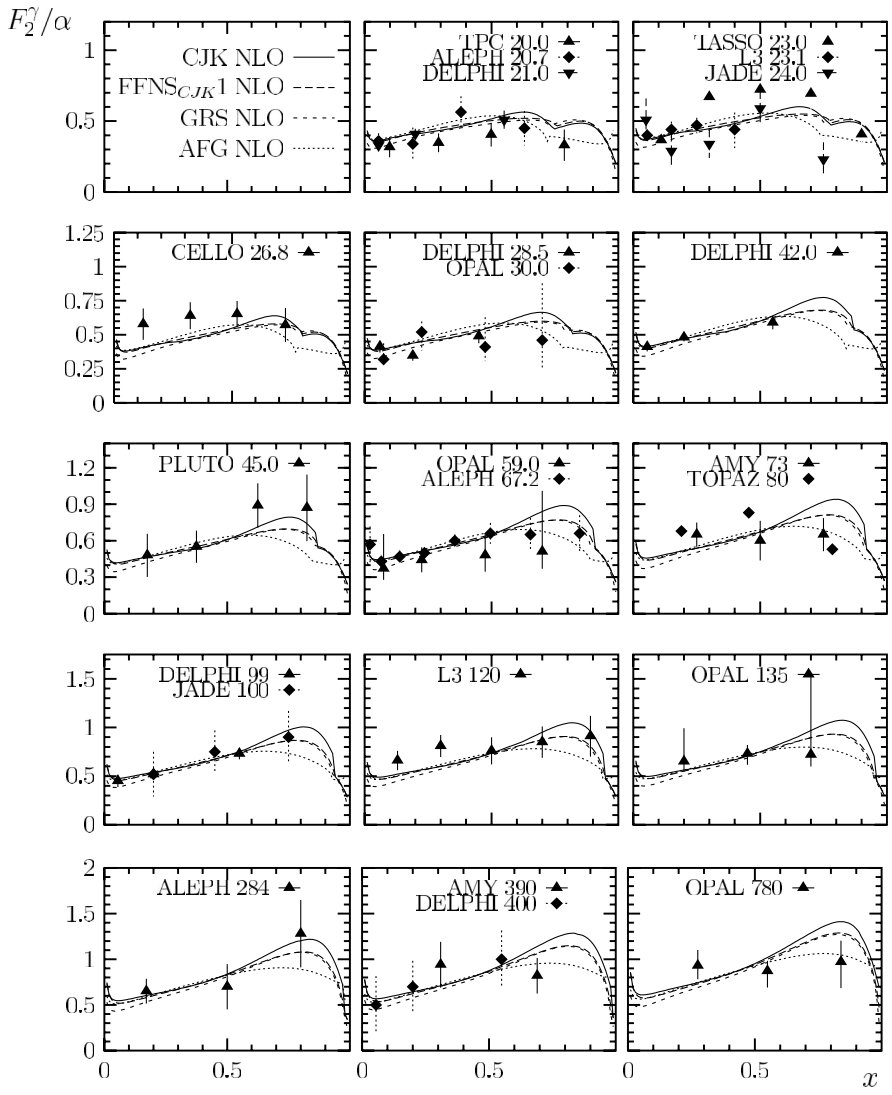

FIG. 9. The same as in Fig. 7 for a linear scale in x.

$$F_{2,c}^\gamma(x,Q^2) = 2xe_c^2 c^\gamma(x,Q^2) + F_{2,c}^\gamma|_{\rm dir}(x,Q^2) + F_{2,c}^\gamma|_{\rm res}(x,Q^2) - F_{2,c}^\gamma|_{\rm res,sub}(x,Q^2) + [2c * C_{2,q}^{(1)}](x,Q^2), \tag{50}$$

with

$$F_{2,c}^\gamma|_{\rm dir}(x,Q^2) = 3xe_c^4\frac{\alpha}{\pi}\left\{-\beta x(1-x)\frac{4m_c^2}{Q^2} + \left[x(1-3x)\times\frac{4m_c^2}{Q^2} - x^2\frac{8m_c^4}{Q^4}\right]\ln\frac{1+\beta}{1-\beta}\right\},$$
$$F_{2,c}^\gamma|_{\rm res}(x,Q^2) = xe_c^2\frac{\alpha_s(Q^2)}{2\pi}\times\int_{\chi_c}^1\frac{dy}{y}G^\gamma(y,Q^2)C_{2,G}^{h,(1)}\left(\frac{x}{y},\frac{Q^2}{m_c^2}\right), \tag{51}$$

$$F_{2,c}^\gamma|_{\rm res,sub}(x,Q^2) = xe_c^2\frac{\alpha_s(Q^2)}{2\pi}\ln\frac{Q^2}{Q_0^2}\times 2\int_{\chi_c}^1\frac{dy}{y}G^\gamma(y,Q^2)P_{qG}^{(0)}\left(\frac{\chi_c}{y}\right),$$
$$[2c * C_{2,q}^{(1)}](x,Q^2) = xe_c^2\frac{\alpha_s(Q^2)}{2\pi}\int_x^1\frac{dy}{y}\times(c^\gamma+\bar{c}^\gamma)(y,Q^2)C_{2,q}^{(1)}\left(\frac{x}{y}\right).$$

Let us stress that the above direct contribution effectively includes both the direct and the direct subtraction terms, as discussed in detail in Sec. IV D. Therefore, it is not the same as the $F_{2,c}^\gamma|_{\rm dir}(x,Q^2)$ in the LO analyses. That way in the NLO analysis we removed the troublesome subtraction term $\sim k_q^{(0)}$. Unfortunately, also the $2c * C_{2,q}^{(1)}$ contribution does not vanish at the threshold and therefore an additional constraint $2c * C_{2,q}^{(1)} = 0$ for $\chi_c > 1$ is neces-

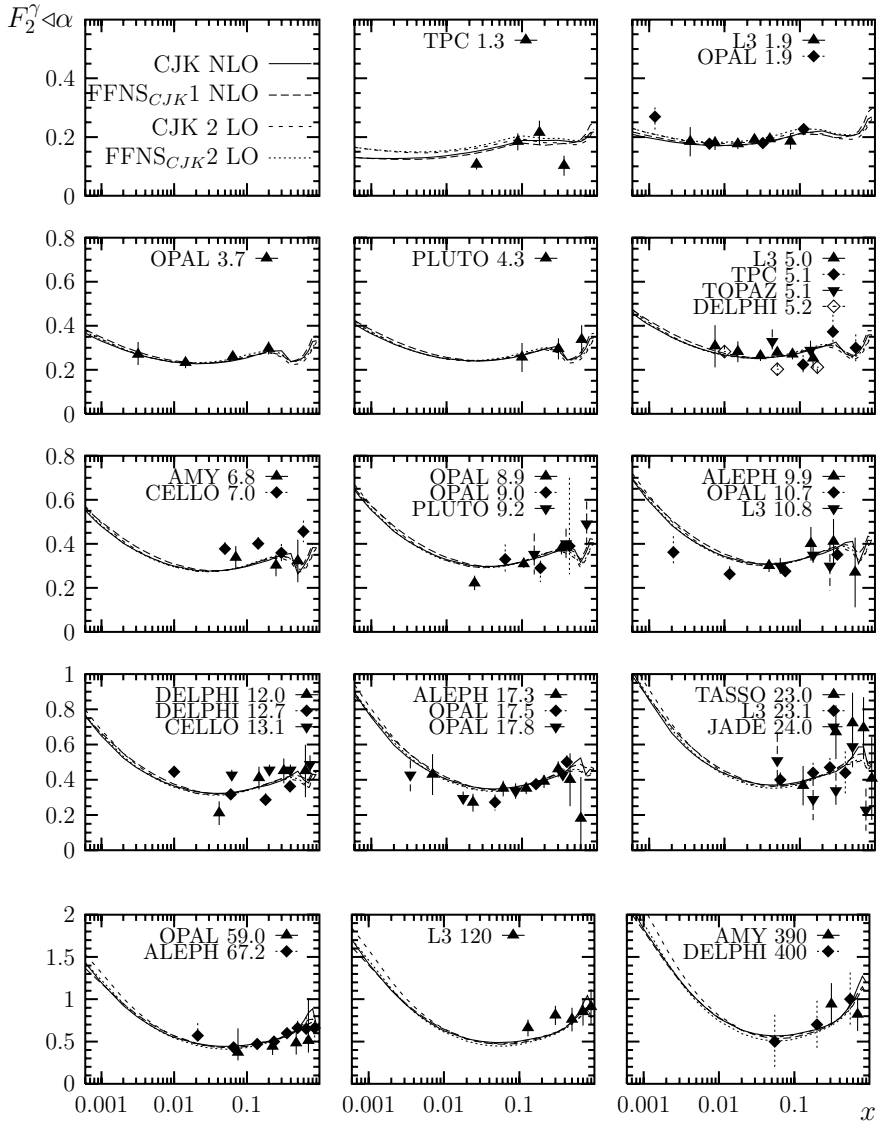

FIG. 10. Predictions for the $F_2^\gamma(x, Q^2)/\alpha$ for the CJK NLO and FFNS$_{\rm CJK}$ NLO models compared with corresponding LO fits from [2] and with the experimental data [25–38], for small and medium Q^2 as a function of x (logarithmic scale). If a few values of Q^2 are displayed in the panel, the average of the smallest and biggest Q^2 was taken in the computation.

sary. This term is important in the high and medium x, its values in the latter range are negative. As can be seen in the plot all other terms vanish in the $W \to 2m_c$ threshold. The direct term influences the $F_{2,c}^\gamma$ only in the medium and high x at low-Q^2 range, where it is negative. The charm-quark density contribution, i.e., the term $2xe_c^2 c^\gamma(x, Q^2)$, dominates the $F_{2,c}^\gamma$ in the whole kinematically available x range. In the low-x region also the resolved-photon contributions increase, but they cancel each other.

A good test of the charm-quark contributions is provided by the OPAL measurement of the $F_{2,c}^\gamma$, obtained from the inclusive production of $D^{*\pm}$ mesons in photon-photon collisions [48]. The averaged $F_{2,c}^\gamma$ has been determined in two x bins. These data points are compared to the predictions of the CJK and FFNS$_{\rm CJK}$1 NLO models, as well as of the corresponding CJK and FFNS$_{\rm CJK}$2 LO models in Fig. 20. The CJK NLO model seems to give the best description of the data, especially for the high-x bin. The FFNS-type models predict the same $F_{2,c}^\gamma$ at $x > 0.03$, while below that value the FFNS$_{\rm CJK}$2 LO predicts higher $F_{2,c}^\gamma$ which finally becomes very similar to the NLO results.

D. Test of importance of $O(\alpha_s^2)$ and $O(\alpha\alpha_s)$ terms

In this section we would like to present the results of the fit of the FFNS$_{\rm CJK}$2 NLO model to the data. As discussed in Secs. III B and III D, in this approach we include the $O(\alpha_s^2)$ and $O(\alpha\alpha_s)$ contributions to the photon structure function:

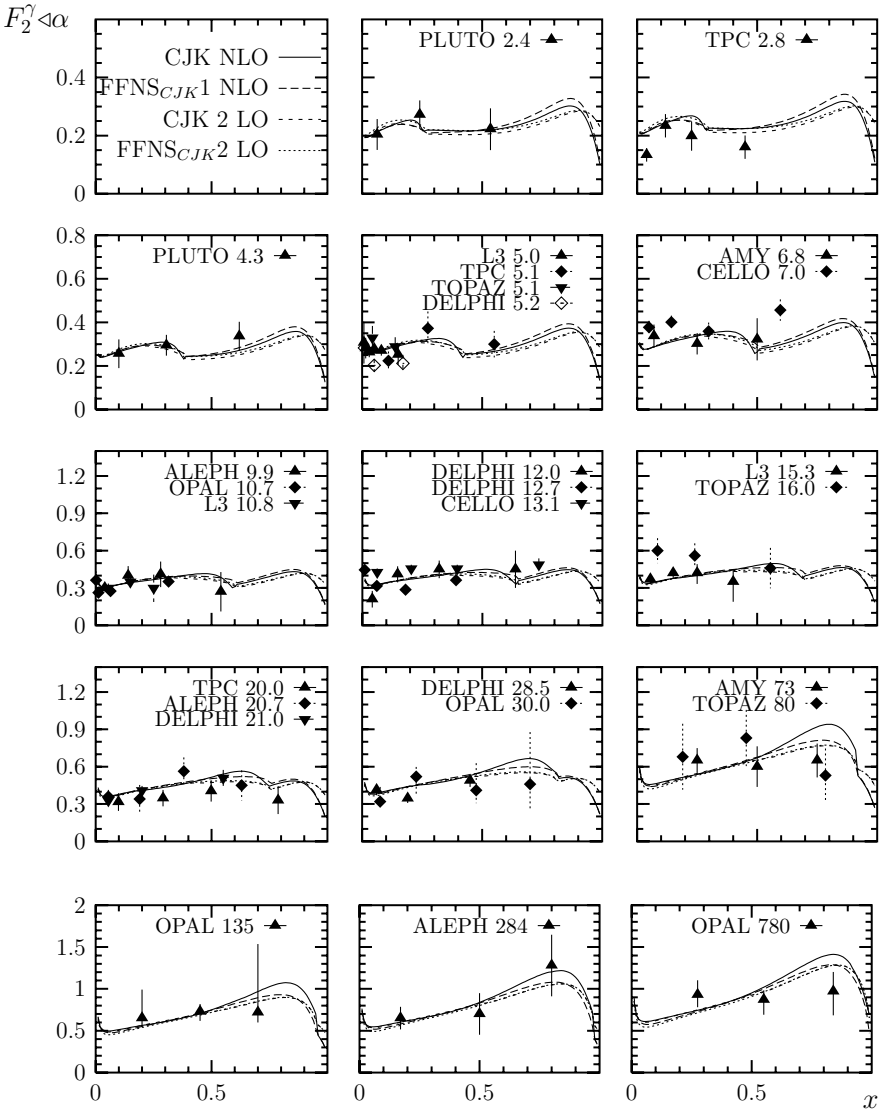

FIG. 11. The same as in Fig. 10 for a linear scale in x.

$$\frac{1}{x}F_2^\gamma(x,Q^2)|_{\text{higher order}} = \sum_{h(=c,b)}^{2}\left\{\left(\frac{\alpha_s(Q^2)}{2\pi}\right)^2\int_{\chi_h}^1\frac{dy}{y}\left[\sum_{i=1}^{3}(q_i^\gamma+\bar{q}_i^\gamma)(y,Q^2)\left(e_i^2C_{2,q}^{(2)}\left(\frac{x}{y},\frac{Q^2}{m_h^2}\right)+e_h^2C_{2,q}^{h,(2)}\left(\frac{x}{y},\frac{Q^2}{m_h^2}\right)\right)\right.\right.$$
$$\left.\left.+e_h^2G^\gamma(y,Q^2)C_{2,G}^{h,(2)}\left(\frac{x}{y},\frac{Q^2}{m_h^2}\right)\right]+\frac{\alpha\alpha_s(Q^2)}{(2\pi)^2}e_h^4C_{2,\gamma}^{h,(1)}\left(x,\frac{Q^2}{m_h^2}\right)\right\}. \quad (52)$$

Alike in the main CJK and FFNS$_{\text{CJK}}$1 NLO models our fit was performed in two steps. First, we treated Q_0^2 as a free parameter in order to obtain better agreement with the data, next it was fixed to the estimated value, $Q_0^2 = 0.716\,\text{GeV}^2$, and a final fit was done. Its results are presented in Table V; all errors were obtained from MINOS requiring $\Delta\chi^2 = 1$.

First let us compare the results of the two FFNS$_{\text{CJK}}$ NLO models, given in Tables IV and V, respectively. We notice that higher $\chi^2/_{\text{d.o.f.}}$ is obtained in the model including additional terms. Next, the input scale and the parameters obtained in both approaches are very similar. The largest distinction is observed between the κ values and can be explained by the small difference between the Q_0^2 values (0.716 and 0.786 GeV^2, respectively). Namely, when we start the evolution of the parton densities at a lower input scale then smaller input distributions are required in order to obtain the same results at the given Q^2.

Further, we compare results computed using four various FFNS$_{\text{CJK}}$ models, the NLO ones described in this work as well as the FFNS$_{\text{CJK}}$1 and two LO models,

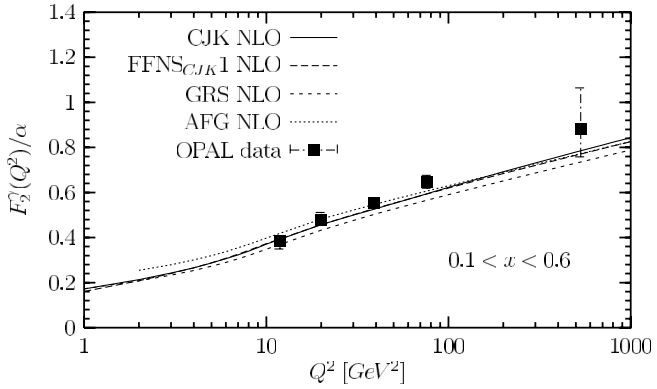

FIG. 12. Comparison of the OPAL data [38] for the Q^2 dependence of the averaged over $0.1 < x < 0.6$ F_2^γ/α with the predictions of the CJK NLO and FFNS$_{\rm CJK}$ NLO models.

presented in [2]. The main differences among the four models, apart from the different order of the QCD DGLAP equations applied, lie in the heavy-quark contributions to F_2^γ. Those differences are summarized in Table VI where all included or excluded terms proportional to Wilson-coefficient functions are listed.

In Fig. 21 we show the parton densities computed in the FFNS$_{\rm CJK}$ models obtained in LO and NLO. A small difference between the LO results seen in Fig. 21 only at small x may be explained by the fact that in that case the models differ only by the resolved-type $\sim C_{2,G}^{h,(1)}$ contribution, which plays an important role only in the low-x region. However, there exist important differences between the two NLO fits, observed especially in the up- and down-quark distributions, which indicate the importance of the higher order $O(\alpha_s^2)$ and $O(\alpha\alpha_s)$ contributions to $F_2^\gamma(x, Q^2)$ at medium x. The distinctions between the

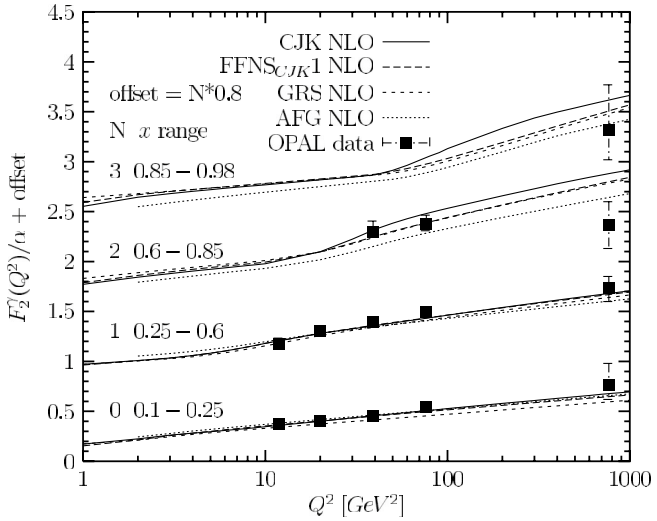

FIG. 13. As in Fig. 12 for $F_2^\gamma(x, Q^2)/\alpha$, averaged over four different x ranges.

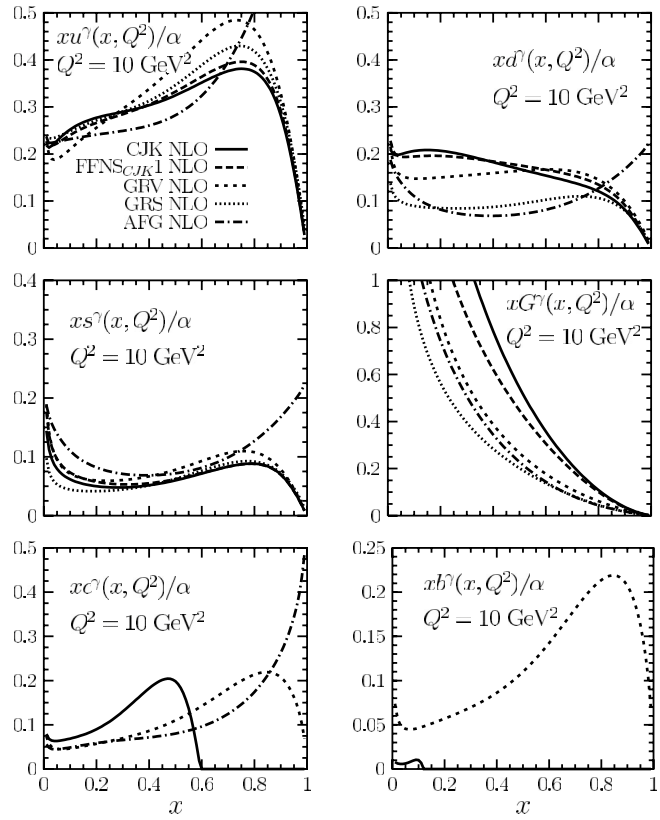

FIG. 14. Comparison of the NLO parton densities predicted by CJK NLO and FFNS$_{\rm CJK}$1 NLO models and by GRV NLO [9], GRS NLO [10], and AFG NLO [47] parametrizations at $Q^2 = 10$ GeV^2, as a function of x.

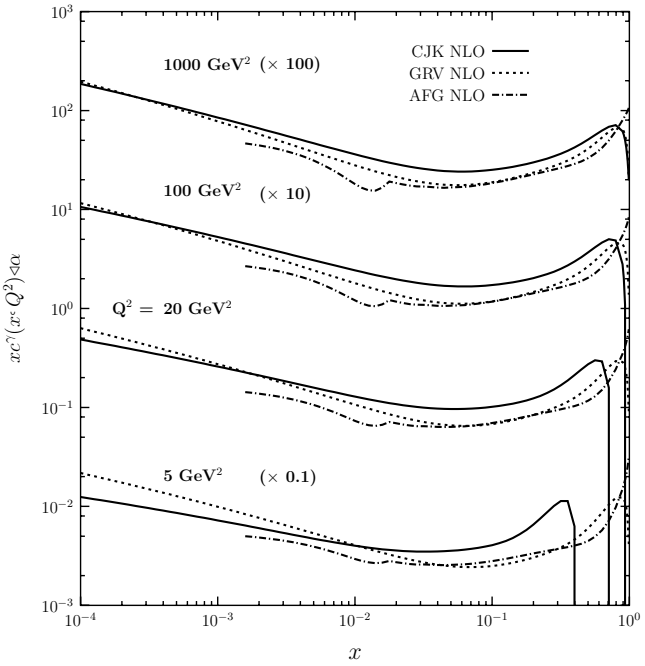

FIG. 15. Comparison of the charm-quark density at four values of Q^2 in the CJK and FFNS$_{\rm CJK}$1 NLO models with the GRV NLO [9], GRS NLO [10], and AFG NLO [47] densities.

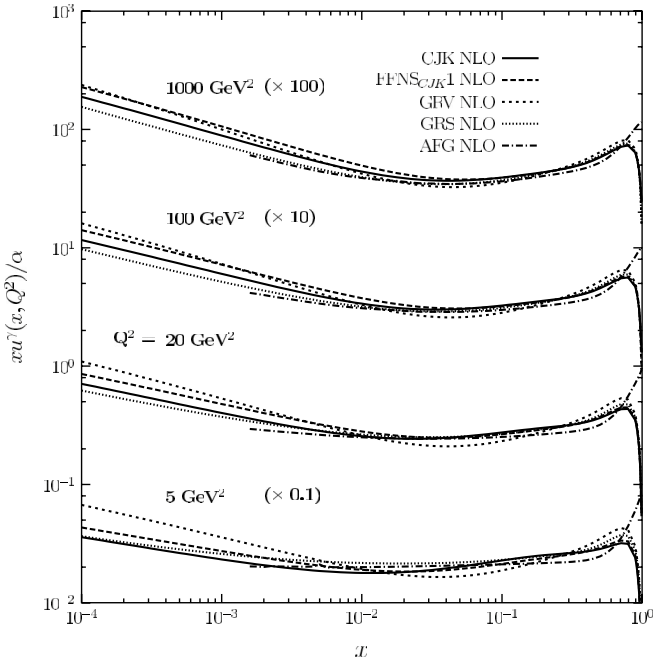

FIG. 16. The same as in Fig. 15 for the up-quark density.

pairs of LO and NLO lines are large at high x where, as discussed before, the NLO distributions decrease much earlier. The maximal values of the NLO u^γ and s^γ distributions are reached at smaller x, $x \sim 0.75$ than in the LO case where the corresponding x value is $x \sim 0.95$. Note however that some other changes such as of the factorization scale or heavy-quark masses may introduce additional differences between LO and NLO fits [10].

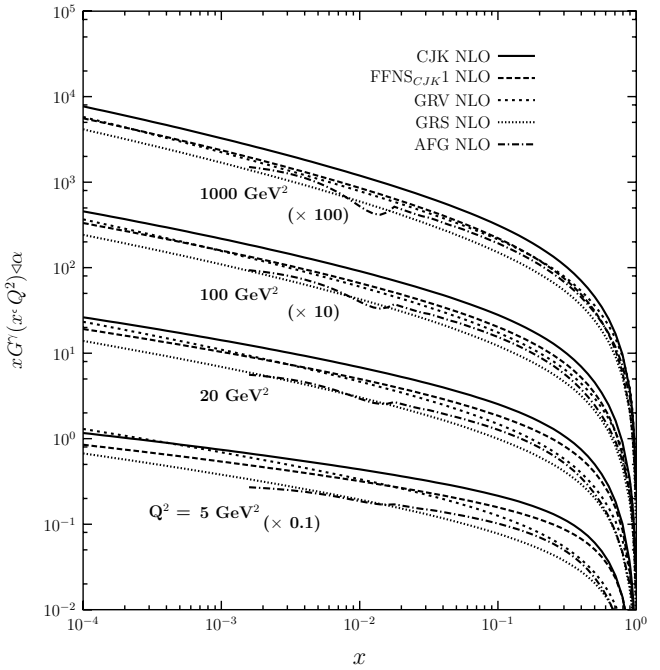

FIG. 17. The same as in Fig. 15 for the gluon density.

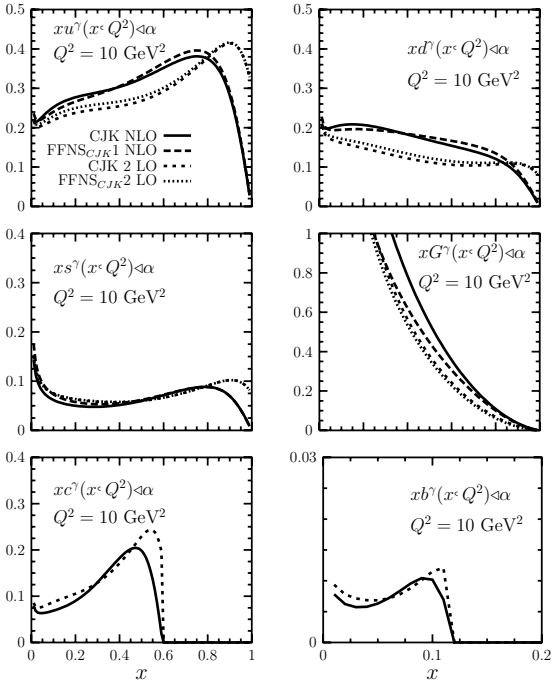

FIG. 18. Comparison of the parton densities predicted by the CJK NLO and FFNS$_{\mathrm{CJK}}$1 NLO models and by corresponding LO models, CJK LO and FFNS$_{\mathrm{CJK}}$2 LO (i.e., including the resolved-photon $\gamma^* G \to h\bar{h}$ contribution) from [2] at $Q^2 = 10$ GeV^2, as a function of x.

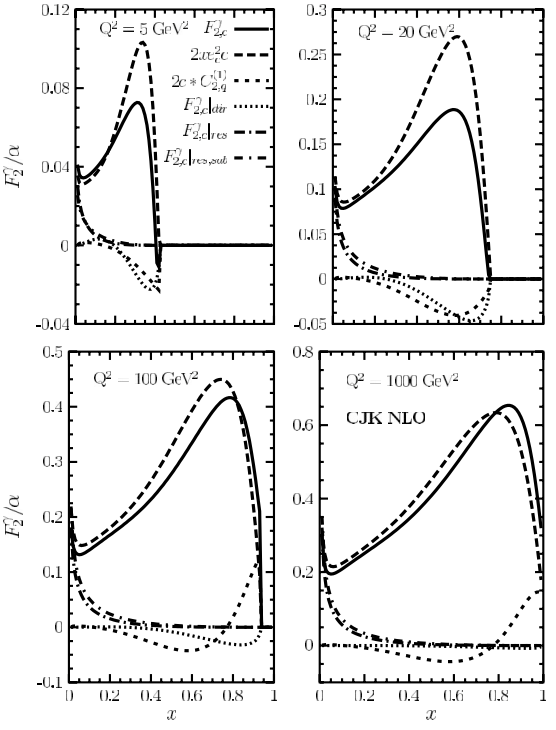

FIG. 19. Comparison of various contributions to the photon structure function $F_{2,c}^\gamma(x, Q^2)/\alpha$ in the CJK NLO model for $Q^2 = 5$, 20, 100, and 1000 GeV^2.

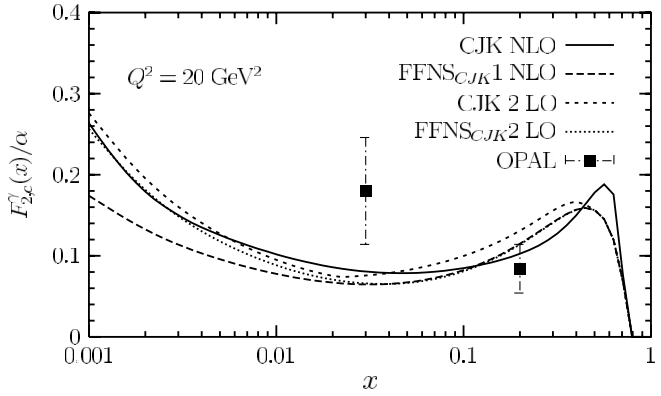

FIG. 20. Comparison of the structure function $F_{2,c}^{\gamma}(x, Q^2)/\alpha$ calculated in the CJK and FFNS$_{\rm CJK}$ models for NLO and LO with the OPAL measurement [48].

E. Influence of the DELPHI LEP2 data

Finally we tested the possible influence of the recent DELPHI data [33], which were not included in the final fits on the results of our models. We performed test fits for the CJK NLO model including separately each of the sets of the LEP2 data obtained with TWOGAM [42], PHOJET [43], and PYTHIA [44] Monte Carlo generators and presented in [33]. As can be seen in Figs. 22 and 23 for the choice of the $F_2^{\gamma}(x, Q^2)$ distributions and the parton densities computed at $Q^2 = 10$ GeV^2, respectively, the results of those fits are very similar to the expectations of the final CJK NLO fit (denoted as "no LEP2"). Still, the $\chi^2/_{\rm d.o.f.}$ obtained in the test fits are much worse; see Table VII.

VII. DISCUSSION AND CONCLUSIONS

A new analysis of the radiatively generated parton distributions in the real photon based on the NLO DGLAP equations is presented. An updated set of the $F_2^{\gamma}(x, Q^2)$ data including recent ALEPH as well as new preliminary DELPHI measurements has been used to perform three global fits. Our models are based on two schemes, the fixed flavor-number scheme and variable flavor-number scheme [ACOT(χ)] which were already applied in our former LO analysis; see [1–3]. We observe that in comparison to the LO models a higher input scale of the NLO DGLAP evolution is required in order to satisfactory describe the data. Further, unlike in the LO case we obtained lower $\chi^2/_{\rm d.o.f.}$ in the FFNS-type approach than in the CJK model. The test fits showed that a

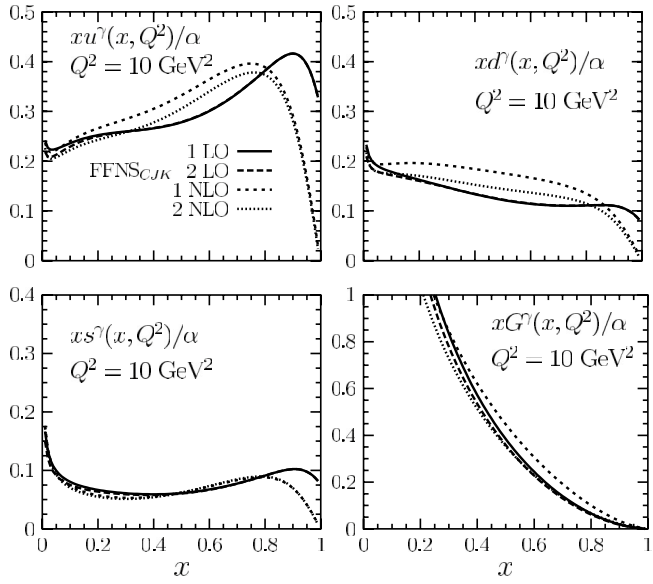

FIG. 21. Comparison of the parton densities predicted by the FFNS$_{\rm CJK}$1 and two NLO models and by the corresponding FFNS$_{\rm CJK}$1 and two LO models presented in [2] at $Q^2 = 10$ GeV^2, as a function of x.

TABLE V. The χ^2 and parameters of the fit for the FFNS$_{\rm CJK}$2 NLO model with assumed $Q_0^2 = 0.716$ GeV^2. The α, β and κ symmetric parabolic errors obtained from MINOS requiring $\Delta\chi^2 = 1$.

NLO model	χ^2	$\chi^2/_{\rm d.o.f.}$	κ	α	β	N_v	$\tilde{N}_G$
FFNS$_{\rm CJK}$2	252.2	1.31	$1.892^{+0.101}_{-0.090}$	$0.527^{+0.089}_{-0.080}$	$0.966^{+0.387}_{-0.333}$	0.797	2.727

TABLE VI. The heavy-quark terms proportional to the Wilson-coefficient functions contributing (or not) to the heavy-quark structure function in various FFNS$_{\rm CJK}$ models.

FFNS$_{\rm CJK}$ model	$C_{2,\gamma}^{h,(0)}$	$C_{2,G}^{h,(1)}$	$C_{2,\gamma}^{h,(1)}$	$C_{2,G}^{h,(2)}$	$C_{2,q}^{h,(2)}$	$C_{2,q}^{(2)}$
LO 1	+	−	−	−	−	−
LO 2	+	+	−	−	−	−
NLO 1	+	+	−	−	−	−
NLO 2	+	+	+	+	+	+

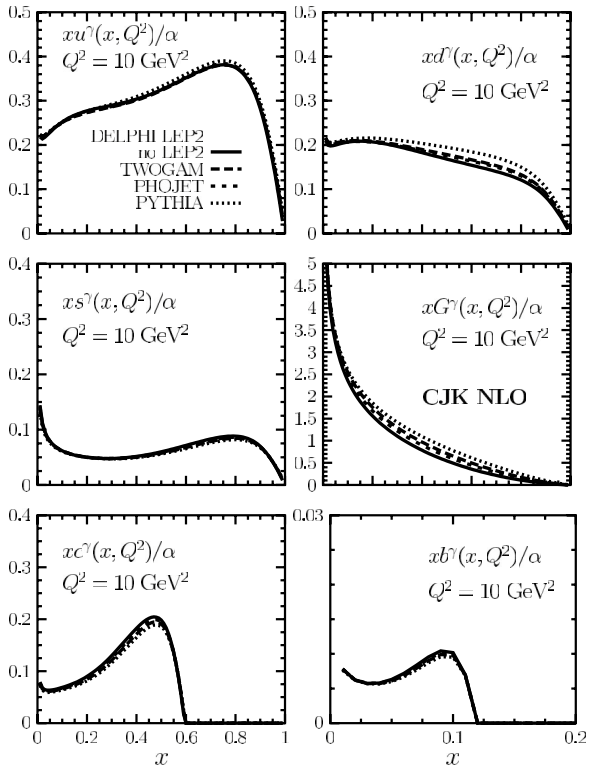

FIG. 22. Comparison of the parton densities predicted by the test fits obtained with the CJK NLO model using various sets of the DELPHI LEP2 data [33] at $Q^2 = 10$ GeV^2, as a function of x.

change of the simple form of the input parton distributions applied in [1–3] and in this work does not lead to the improvement of the fits.

Predictions of the FFNS$_{\rm CJK}$1 and CJK NLO fits are compared with the $F_2^\gamma(x, Q^2)$ data, other parametrizations, and corresponding LO models. Both models describe very well the Q^2 evolution of the $F_2^\gamma(x, Q^2)$, averaged over various x regions. The $F_{2,c}^\gamma$ calculated in the CJK NLO model gives best agreement with the data.

TABLE VII. Number of experimental points used in the test fits for the CJK NLO model and the resulting χ^2.

Set	χ^2	No. of points	$\chi^2/_{\rm d.o.f.}$
TWOGAM	307.4	209	1.50
PHOJET	312.0	207	1.54
PYTHIA	341.1	209	1.66

Next, we check the difference between the results obtained in the FFNS$_{\rm CJK}$1 NLO model and the FFNS$_{\rm CJK}$2 NLO model which includes additional $O(\alpha_s^2)$ and $O(\alpha\alpha_s)$ contributions to $F_2^\gamma(x, Q^2)$. Those higher order terms prove to be of importance. Therefore, further studies of the CJK model including terms of the same order are required.

Finally, we examine the influence on the results of our models of the various sets of the LEP2 data presented in the recent preliminary results of the DELPHI Collaboration but excluded from final fits. Test fits show a very small change of the $F_2^\gamma(x, Q^2)$ and parton distributions obtained using these data comparing to the final fits but a large deterioration of their quality.

FORTRAN parametrization programs for our CJK and FFNS$_{\rm CJK}$ NLO models can be obtained from the web page [49].

APPENDIX: THE WILSON-COEFFICIENT FUNCTIONS

Lists of all Wilson-coefficient functions used in this analysis are given in Tables I and II. The Wilson coefficients $C_{2,q}^{(1)}$, $C_{2,G}^{(1)}$, and $C_{2,\gamma}^{(0)}$ have been first calculated in

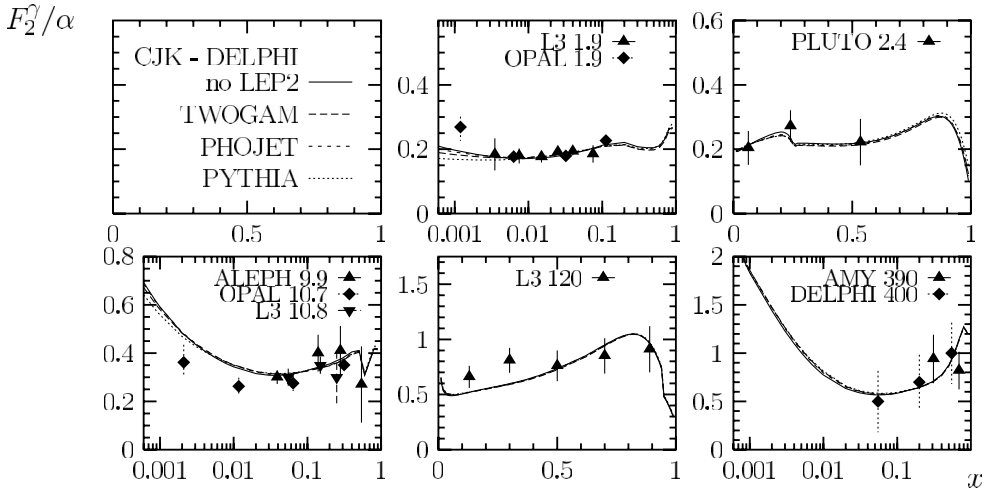

FIG. 23. Predictions for the $F_2^\gamma(x, Q^2)/\alpha$ for the CJK NLO model obtained in the test fits using various sets of the DELPHI LEP2 data [33].

the operator product expansion [50] in the Mellin space in the articles [51,52], respectively. In the (x, Q^2) space the $C_{2,\gamma}^{(0)}$ in the $\overline{\rm MS}$ factorization scheme reads (see for instance [10])

$$C_{2,\gamma}^{(0)}(x) = 6\left\{-1 + 8x(1-x) + [x^2 + (1-x)^2]\ln\frac{1-x}{x}\right\}. \tag{A1}$$

The lowest order heavy-quark coefficient $C_{2,\gamma}^{h,(0)}$, given by the Bethe-Heitler $\gamma^* + \gamma \to q + \bar{q}$ process, has been first presented in [53]. It has the following form:

$$C_{2,\gamma}^{h,(0)}\left(x, \frac{Q^2}{m_h^2}\right) = 6\left\{\beta\left[-1 + 8x(1-x) - x(1-x)\frac{4m_h^2}{Q^2}\right] + \ln\left(\frac{1+\beta}{1-\beta}\right)\left[x^2 + (1-x)^2 + x(1-3x)\times\frac{4m_h^2}{Q^2} - x^2\frac{8m_h^4}{Q^4}\right]\right\}, \tag{A2}$$

with $\beta = \sqrt{1 - [4m_h^2 x/(1-x)Q^2]}$.

When we neglect the heavy-quark mass in some parts of the coefficient $C_{2,\gamma}^{h,(0)}$ we can rewrite it as in Eq. (21)

$$C_{2,\gamma}^{h,(0),\overline{\rm MS}}\left(x, \frac{Q^2}{m_h^2}\right) \approx C_{2,\gamma}^{(0),\overline{\rm MS}}(x) + 2k_q^{(0),\overline{\rm MS}}(x)\ln\frac{Q^2}{m_h^2} + 6\left\{-\beta x(1-x)\frac{4m_h^2}{Q^2} + \left[x(1-3x)\times\frac{4m_h^2}{Q^2} - x^2\frac{8m_h^4}{Q^4}\right]\ln\frac{1+\beta}{1-\beta}\right\}, \tag{A3}$$

where the direct-photon-quark splitting function is

$$k_q^{(0)} = 3[x^2 + (1-x)^2]. \tag{A4}$$

The $C_{2,G}^{h,(1)}$ function related to the $\gamma^* + G \to q + \bar{q}$ process reads

$$C_{2,G}^{h,(1)}\left(x, \frac{Q^2}{m_h^2}\right) = \frac{1}{6}C_{2,\gamma}^{h,(0)}\left(x, \frac{Q^2}{m_h^2}\right) = \beta\left[-1 + 8x(1-x) - x(1-x)\frac{4m_h^2}{Q^2}\right] + \ln\left(\frac{1+\beta}{1-\beta}\right)\left[x^2 + (1-x)^2 + x(1-3x)\frac{4m_h^2}{Q^2} - x^2\frac{8m_h^4}{Q^4}\right]. \tag{A5}$$

Finally, the higher order heavy-quark coefficients, $C_{2,\gamma}^{h,(1)}$, $C_{2,G}^{(2)}$, $C_{2,q}^{h,(2)}$, and $C_{2,q}^{(2)}$, are calculated in a series of publications [15]. They are given in the form of a two dimensional array. Those $O(\alpha_s^2)$ and $O(\alpha\alpha_s)$ order Wilson coefficients are given as

$$C_{2,i}^{h,(k)}(x, m_h^2, Q^2, \mu^2) = C_{2,i}^{h,(k)}\left(x, \frac{Q^2}{m_h^2}\right) + \bar{C}_{2,i}^{h,(k)}\left(x, \frac{Q^2}{m_h^2}\right)\ln\frac{\mu^2}{m_h^2}, \tag{A6}$$

where μ^2 is the mass factorization scale. In our calculations we simplify the above formula by choosing $\mu^2 = m_h^2$.

ACKNOWLEDGMENTS

P. J. would like to thank E. Laenen for making accessible the formulas for the Wilson coefficients and for his comments. Moreover, P. J. is grateful to I. Schienbein for his help in obtaining correct NLO DGLAP evolution programs. We want to thank R. Gokieli and K. Doroba for their comments on the recent DELPHI data. Finally P. J. is grateful to M. Aurenche and M. Fontannaz for the AFG parametrization program, R. Nisius for all his remarks concerning the experimental data, and A. Zembrzuski for his comments. This work was partly supported by the European Community's Human Potential Programme under Contract No. HPRN-CT-2000-00149 Physics at Collider and HPRN-CT-2002-00311 EURIDICE. F. C. also acknowledges partial financial support from Ministerio de Ciencia y Tecnología under Project No. FPA2003-09298-c02-01 and Junta de Andalucía under Project No. FQM 330. This work was partially supported by the Polish Committee for Scientific Research, Grant No. 1 P03B 040 26 and Project No. 115/E-343/SPB/DESY/P-03/DWM517/2003-2005.

[1] F. Cornet, P. Jankowski, M. Krawczyk, and A. Lorca, Phys. Rev. D **68**, 014010 (2003).

[2] F. Cornet, P. Jankowski, and M. Krawczyk, IFT Report No. IFT-2003-30, 2003; Nucl. Phys. B, Proc. Suppl. **126**, 28 (2004).

[3] P. Jankowski, J. High Energy Phys. 05 (2004) 055.

[4] These two $\text{FFNS}_{\text{CJK}}1$ and 2 models differ from the corresponding models introduced in our LO analysis.

[5] S. Kretzer, C. Schmidt, and W. Tung, J. Phys. G **28**, 983 (2002); S. Kretzer, H. L. Lai, F. I. Olness, and W. K. Tung, Phys. Rev. D **69**, 114005 (2004).

[6] Inclusion of the $O(\alpha_s^2)$ terms in the CJK NLO approach is beyond the scope of this work.

[7] M. Glück, E. Reya, and A. Vogt, Z. Phys. C **53**, 127 (1992).

[8] M. Glück, E. Reya, and A. Vogt, Z. Phys. C **53**, 651 (1992).

[9] M. Glück, E. Reya, and A. Vogt, Phys. Rev. D **46**, 1973 (1992).

[10] M. Glück, E. Reya, and I. Schienbein, Phys. Rev. D **60**, 054019 (1999); **62**, 019902(E) (2000).

[11] M. Glück, E. Reya, and M. Stratmann, Phys. Rev. D **51**, 3220 (1995).

[12] S. Albino, M. Klasen, and S. Söldner-Rembold, Phys. Rev. Lett. **89**, 122004 (2002).

[13] A. Chuvakin, J. Smith, and W. L. van Neerven, Phys. Rev. D **61**, 096004 (2000).

[14] A. Chuvakin, J. Smith, and W. L. van Neerven, Phys. Rev. D **62**, 036004 (2000).

[15] E. Laenen, S. Riemersma, J. Smith, and W. L. van Neerven, Nucl. Phys. **B392**, 162 (1993); Phys. Lett. B **291**, 325 (1992); Phys. Rev. D **49**, 5753 (1994); S. Riemersma, J. Smith, and W. L. van Neerven, Phys. Lett. B **347**, 143 (1995).

[16] G. Parisi, Nucl. Phys. **B126**, 298 (1997).

[17] R. K. Ellis, W. J. Stirling, and B. R. Weber, *QCD and Collider Physics* (Cambridge Univerity Press, Cambridge, 1996).

[18] M. Glück, E. Reya, and A. Vogt, Phys. Rev. D **45**, 3986 (1992).

[19] A. Vogt, Ph.D. thesis, Dortmund University, 1992 (Report No. DO-TH-92-15).

[20] Notice that we neglected the Q^2 dependence of the strong coupling α_s and the gluon density $G(y, Q^2)$.

[21] E. G. Floratos, C. Kounnas, and R. Lacaze, Nucl. Phys. **B192**, 417 (1981).

[22] J. H. Field, in *Proceedings of the VIIIth International Workshop on Photon-Photon Collisions, Shoresh, Jerusalem Hills, Israel, 1988* (World Scientific, Singapore, 1988); U. Maor, Acta Phys. Pol. B **19**, 623 (1988); Ch. Berger and W. Wagner, Phys. Rep. **146**, 1 (1987).

[23] Particle Data Group, D. E. Groom *et al.*, Eur. Phys. J. C **15**, 1 (2000).

[24] J. C. Collins and W. Tung, Nucl. Phys. **B278**, 934 (1986).

[25] CELLO Collaboration, H. J. Behrend *et al.*, Phys. Lett. **126B**, 391 (1983); in *Proceedings of the XXVth International Conference on High Energy Physics, Singapore, 1990*, edited by K. K. Phua and Y. Yamaguchi (World Scientific, Singapore, 1991).

[26] PLUTO Collaboration, Ch. Berger *et al.*, Phys. Lett. **142B**, 111 (1984); Nucl. Phys. **B281**, 365 (1987).

[27] JADE Collaboration, W. Bartel *et al.*, Z. Phys. C **24**, 231 (1984).

[28] TPC/2γ Collaboration, H. Aihara *et al.*, Z. Phys. C **34**, 1 (1987); J. S. Steinman, Ph.D. thesis, UCLA, 1988 (UCLA Report No. UCLA-HEP-88-004, 1988).

[29] TASSO Collaboration, M. Althoff *et al.*, Z. Phys. C **31**, 527 (1986).

[30] TOPAZ Collaboration, K. Muramatsu *et al.*, Phys. Lett. B **332**, 477 (1994).

[31] AMY Collaboration, S. K. Sahu *et al.*, Phys. Lett. B **346**, 208 (1995); T. Kojima *et al.*, *ibid.* **400**, 395 (1997).

[32] DELPHI Collaboration, P. Abreu *et al.*, Z. Phys. C **69**, 223 (1996); I. Tyapkin, in *Proceedings of the Workshop on Photon Interaction and the Photon Structure, Lund, Sweden, 1998*, edited by G. Jarlskog and T. Sjöstrand (CERN, Geneva, 1998).

[33] DELPHI Collaboration, contribution to the Proceedings of the European Physical Society International Europhysics Conference on High Energy Physics, Aachen, Germany, 2003; contribution to the Proceedings of the Lepton Photon 2003 XXI International Symposium on Lepton and Photon Interactions at High Energies, 2003, Fermilab, Batavia, IL [Int. J. Mod. Phys. A **19**, 785 (2004)].

[34] L3 Collaboration, M. Acciarri *et al.*, Phys. Lett. B **436**, 403 (1998); **447**, 147 (1999); **483**, 373 (2000).

[35] ALEPH Collaboration, R. Barate *et al.*, Phys. Lett. B **458**, 152 (1999).

[36] ALEPH Collaboration, A. Heister *et al.*, Eur. Phys. J. C **30**, 145 (2003).

[37] OPAL Collaboration, K. Ackerstaff *et al.*, Z. Phys. C **74**, 33 (1997); Phys. Lett. B **411**, 387 (1997); G. Abbiendi *et al.*, Eur. Phys. J. C **18**, 15 (2000).

[38] OPAL Collaboration, G. Abbiendi *et al.*, Phys. Lett. B **533**, 207 (2002).

[39] ALEPH Collaboration, K. Affholderbach *et al.*, Nucl. Phys. B, Proc. Suppl. **86**, 122 (2000).

[40] DELPHI Collaboration, I. Tyapkin *et al.*, in *Proceedings of the International Conference on the Structure and Interactions of the Photon and 14th International Workshop on Photon-Photon Collisions (Photon 2001), Ascona, Switzerland* (World Scientific, Singapore, 2002).

[41] All LEP2 data are given in three sets obtained with the TWOGAM [42], PHOJET [43], and PYTHIA [44] Monte Carlo generators.

[42] S. Nova, A. Olshevsky, and T. Todorov, Delphi Report No. DELPHI-90-35, 1990 (unpublished).

[43] R. Engel, Z. Phys. C **66**, 203 (1995); R. Engel and J. Ranft, Phys. Rev. D **54**, 4244 (1996), http://www-ik.fzk.de/~engel/phojet.html

[44] *Workshop on Physics at LEP2* (CERN Report No. 96-01, 1996), Vol. 2.

[45] F. James and M. Roos, Comput. Phys. Commun. **10**, 343 (1975).

[46] For test fits we applied MIGRAD instead of MINOS which requires much more computer time.

[47] P. Aurenche, J.-P. Guillet, and M. Fontannaz, Z. Phys. C **64**, 621 (1994).

[48] OPAL Collaboration, G. Abbiendi *et al.*, Phys. Lett. B **539**, 13 (2002).

[49] http://www.fuw.edu.pl/~pjank/param.html

[50] K. G. Wilson, Phys. Rev. **179**, 1499 (1969).

[51] W. A. Bardeen, A. J. Buras, D.W. Duke, and T. Muta, Phys. Rev. D **18**, 3998 (1978).

[52] W. A. Bardeen and A. J. Buras, Phys. Rev. D **20**, 166 (1979); **21**, 2041(E) (1980).

[53] E. Witten, Nucl. Phys. **B104**, 445 (1976); M. Glück and E. Reya, Phys. Lett. **83B**, 98 (1979).